JGR Oceans

RESEARCH ARTICLE
10.1029/2020JC016113

Control of the Oceanic Heat Content of the Getz-Dotson Trough, Antarctica, by the Amundsen Sea Low

Tiago S. Dotto[1,2], Alberto C. Naveira Garabato[1], Anna K. Wåhlin[3], Sheldon Bacon[4], Paul R. Holland[5], Satoshi Kimura[6], Michel Tsamados[7], Laura Herraiz-Borreguero[8], Ola Kalén[3,9], and Adrian Jenkins[5,10]

[1]Ocean and Earth Science, University of Southampton, Southampton, UK, [2]Laboratório de Estudos dos Oceanos e Clima, Instituto de Oceanografia, Universidade Federal do Rio Grande, Rio Grande, Brazil, [3]Department of Marine Sciences, University of Gothenburg, Gothenburg, Sweden, [4]National Oceanography Centre, Southampton, UK, [5]British Antarctic Survey, Cambridge, UK, [6]Japan Agency for Marine-Earth Science and Technology, Yokosuka, Japan, [7]Centre for Polar Observation and Modelling, Department of Earth Sciences, University College London, London, UK, [8]Commonwealth Scientific and Industrial Research Organisation Oceans and Atmosphere and Centre for Southern Hemisphere Oceans Research, Hobart, Tasmania, Australia, [9]Swedish Meteorological and Hydrological Institute, Gothenburg, Sweden, [10]Now at Department of Geography and Environmental Sciences, Northumbria University, Newcastle upon Tyne, UK

Key Points:
- Circumpolar Deep Water inflow to the Getz-Dotson Trough, Amundsen Sea, is investigated with a multiyear mooring
- On-shelf heat content decreased between 2010 and 2015 in response to weaker Circumpolar Deep Water inflow
- Getz-Dotson Trough cooling is driven by a westward wind anomaly at the shelf break, associated with a deeper Amundsen Sea Low

Correspondence to:
T. S. Dotto,
tiagosdotto@gmail.com

Citation:
Dotto, T. S., Naveira Garabato, A. C., Wåhlin, A. K., Bacon, S., Holland, P. R., Kimura, S., et al. (2020). Control of the oceanic heat content of the Getz-Dotson Trough, Antarctica, by the Amundsen Sea Low. *Journal of Geophysical Research: Oceans*, *125*, e2020JC016113. https://doi.org/10.1029/2020JC016113

Received 25 JAN 2020
Accepted 25 JUL 2020
Accepted article online 3 AUG 2020

Abstract The changing supply of warm Circumpolar Deep Water (CDW) to the West Antarctic continental shelf is responsible for the basal melting and thinning of the West Antarctic ice shelves that has occurred in recent decades. Here we assess the variability in CDW supply, and its drivers, from a multiyear mooring deployed in, and a regional ocean model spanning, the Getz-Dotson Trough, Amundsen Sea. Between 2010 to 2015, the CDW within the trough underwent a pronounced cooling and freshening, associated with changes in thermohaline properties on isopycnals. Variability in the rate of CDW inflow is controlled by local wind forcing of a shelf break undercurrent, which determines the hydrographic properties of inflowing CDW via tilting of density surfaces above the continental slope. Local wind is coupled to the Amundsen Sea Low (ASL) low-pressure system, which is modulated by large-scale climatic modes via atmospheric teleconnections. For the period analyzed, a deeper ASL was associated with westward wind anomaly at the shelf break. Changes in the sea surface slope decelerated the shelf break undercurrent, resulting in less heat accessing the continental shelf and, consequently, a cooling of the Getz-Dotson Trough. Therefore, the present work suggests that the fate of the West Antarctic ice shelves is closely tied to the future evolution of the ASL.

Plain Language Summary The heat available for the melting of the ice shelves of the Amundsen Sea is supplied by the warm waters flooding the continental shelf. Here we show that the waters flowing into the Getz-Dotson Trough underwent a pronounced cooling between 2010 and 2015, associated with a weakening of the bottom-intensified currents within the trough. This process was controlled by changes of shelf break winds. A weakening of the eastward wind impacts the middepth undercurrent system above the continental slope, which controls the inflow of warm water via tilting of density surfaces above the slope. The local winds are modulated by the low-pressure system located offshore of the Amundsen Sea, known as the Amundsen Sea Low. The Amundsen Sea circulation is controlled by this low-pressure system, and changes in its configuration can impact the warmer waters flooding the West Antarctic continental shelf, with consequences for the melting of the region's ice shelves.

1. Introduction

The West Antarctic Ice Sheet (WAIS) has lost mass at high rates in recent decades (Mouginot et al., 2014; Shepherd et al., 2018) and has been argued to be prone to irreversible retreats and a possible collapse in the future (Joughin et al., 2014; Rignot et al., 2014). By 2017, the WAIS had contributed ~6 mm to global sea level rise (Shepherd et al., 2018); nevertheless, the total freshwater it contains stored as land ice may raise the global sea level by ~5 m if melted (Morlighem et al., 2020).

The thinning of the West Antarctic ice shelves is generally associated with basal melt driven by relatively warm Circumpolar Deep Water (CDW; Paolo et al., 2015). CDW floods the bottom layers in the deep troughs crosscutting the continental shelf and slope and can reach the deep cavities beneath the ice shelves, inducing

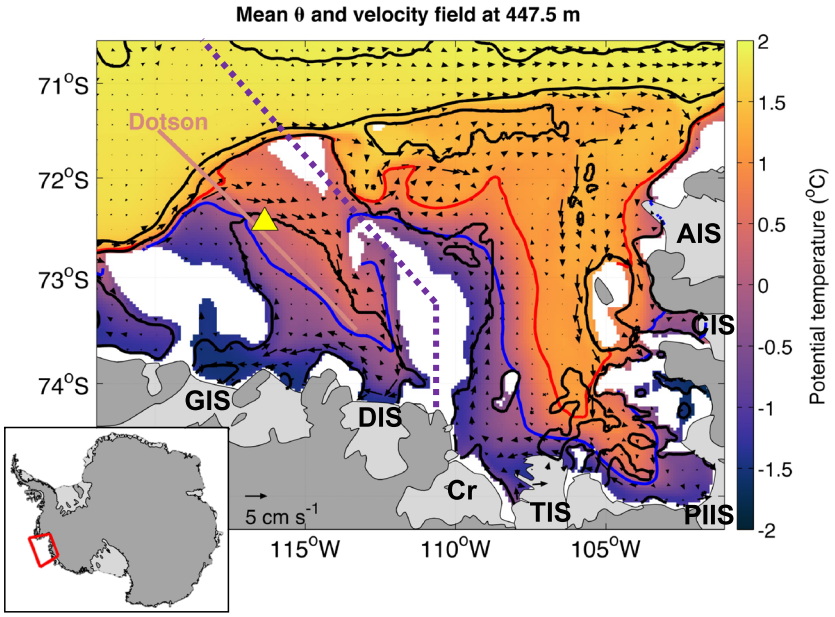

Figure 1. Averaged 1995–2014 potential temperature (θ) and ocean circulation at 447.5 m depth from a regional ocean model (Kimura et al., 2017). The yellow triangle depicts the location of mooring S1. Isobaths of 500, 1,000 and 3,000 m are shown (black lines). Isotherms of 0°C and 1°C are indicated by blue and red lines, respectively. Velocity vectors are plotted every five grid cells. The section crossing the Getz-Dotson Trough is depicted by the light brown line. The purple dotted line splits the region into the Getz-Dotson Trough (to the left) and Pine Island-Thwaites Trough (to the right). Ice shelves (ice sheet) are shown in light (dark) gray. Local ice shelves: Abbot Ice Shelf (AIS), Cosgrove Ice Shelf (CIS), Pine Island Ice Shelf (PIIS), Thwaites Ice Shelf (TIS), Crosson Ice Shelf (Cr), Dotson Ice Shelf (DIS), and Getz Ice Shelf (GIS). Depths shallower than 450 m are masked in white. Inset indicates the study region. Color map from cmocean (Thyng et al., 2016).

a retreat of their grounding lines (Dutrieux et al., 2014; Jenkins et al., 2010; Konrad et al., 2018). In the Amundsen Sea (Figure 1), the CDW that flows into the troughs has temperatures of 2–4°C above the seawater freezing point, and, on its way toward the ice shelves, it can mix with surrounding waters and change its thermohaline properties.

Earlier studies have suggested a relationship between local winds and warm waters flooding the continental shelves off West Antarctica (Kim et al., 2017; Steig et al., 2012; Thoma et al., 2008). Generally, higher temperatures on the continental shelf of the Pine Island-Thwaites Trough (Figure 1) are associated with stronger eastward wind anomalies at the shelf break (Jenkins et al., 2016; Thoma et al., 2008), which are intensified by extratropical climate phenomena (Dutrieux et al., 2014; Holland et al., 2019; Steig et al., 2012). However, there is an ambiguity regarding the process by which the warm waters access the continental shelf. Some studies describe that the eastward wind anomaly over the shelf break directly controls the heat inflow through modification of the local currents in the Getz-Dotson Trough (Wåhlin et al., 2013) and in the Pine Island-Thwaites Trough (Assmann et al., 2013; Thoma et al., 2008; Wåhlin et al., 2012; Walker et al., 2013). Other studies identified that the regional wind pattern, mediated by the sea ice cover, creates Ekman pumping at the shelf break that brings deeper, warmer waters onto the continental shelf. This has been observed in the Getz-Dotson Trough (Assmann et al., 2019; Kim et al., 2017; Kimura et al., 2017) as well as in the Pine Island-Thwaites Trough (Kimura et al., 2017; Webber et al., 2019). However, oceanographic records remain sparse, and the process by which the wind affects the heat content off West Antarctica is still not well understood.

Recently, Dotto et al. (2019) used a regional model to show that bathymetric configuration and thermocline depth also affect the dynamics underpinning the CDW inflow and the proportions of heat that enter the different troughs of the Amundsen Sea (Figure 1). The wind forcing accelerates the eastward slope undercurrent along the slope, delivering CDW that floods the troughs. The eastward slope undercurrent is a

bottom-intensified current located on the continental slope and shelf break of the Amundsen Sea at a depth of ~500 m, beneath the westward Antarctic Slope Current (Walker et al., 2013). Similar features are also described in other regions around Antarctica (Chavanne et al., 2010; Silvano et al., 2019), although their formation processes remain unclear. The undercurrent's eastward flow is diverted poleward where it encounters a trough, creating a cyclonic circulation (Klinck, 1996; St-Laurent et al., 2013). In the Getz-Dotson Trough (Figure 1), the model suggests that variations in on-shelf heat are governed primarily by temperature changes along isopycnals. In contrast, heat perturbations in the Pine Island-Thwaites Trough (Figure 1) are mainly associated with temperature changes due to heaving of isopycnals, where the shallower thermocline allows the access of CDW onto the continental shelf with less mixing with the surrounding water masses (Dotto et al., 2019).

Previous works have documented periods of cooling and warming on the Amundsen Sea continental shelf between the 2000s and the 2010s, with impacts on the melting of ice shelves (Christianson et al., 2016; Dutrieux et al., 2014 ; Jenkins et al., 2018). Decadal variations in the eastward wind intensity at the shelf break were shown to be relevant to these cold/warm oceanic anomalous periods (Holland et al., 2019; Jenkins et al., 2016). In the Pine Island Bay, such transitions have been associated with the phase of El Niño–Southern Oscillation (ENSO). The CDW thickness decreases during La Niña periods and increases during El Niño, mediated by changes in wind forcing (Dutrieux et al., 2014; Steig et al., 2012). Higher melt rates of ice shelves are observed in years when the oceanic heat content in the Amundsen Sea is higher (Dutrieux et al., 2014; Jenkins et al., 2018). However, melting is also modulated on short time scales by highly localized phenomena, such as thermocline depth variations at the ice shelves' calving front (Davis et al., 2018; St-Laurent et al., 2015; Webber et al., 2017).

From the 1920s to the present, the Pine Island Bay shelf break winds may have transitioned from mean easterlies to near-zero mean zonal wind, associated with greenhouse gas forcing (Holland et al., 2019). When superimposed upon this trend, decadal ocean variability, linked to the tropical Pacific influence, created gradually more prevalent oceanic warm anomalies (Holland et al., 2019). The strength and timing of these decadal events might be more influential on the ice shelf configuration than changes in the longer-term mean oceanic state (Holland et al., 2019; Jenkins et al., 2018). Thus, studying these transitional periods and their drivers is essential to comprehend the extent of WAIS stability.

Here we assess the climatic controls of the oceanic heat content of the Getz-Dotson Trough, Amundsen Sea, during a paradigmatic transitional period, by analyzing measurements gathered by a multiyear mooring (Figure 1). The mooring successfully captured quasi-continually a major transition between a warm regime in 2010 and a cold regime in 2015, as previously documented (Jenkins et al., 2018). The oceanic heat reaching the trough is found to be tightly regulated by local wind forcing. The dynamics underpinning the wind's driving of variability in subsurface ocean currents are elucidated with a regional model. Finally, the local atmospheric conditions are shown to be strongly coupled to the Amundsen Sea Low (ASL), the state of which is modulated by large-scale climate variability. This suggests that the fate of the WAIS is closely tied to the future evolution of that low-pressure system.

2. Data and Methods

2.1. Mooring Data

We used a mooring, named S1, deployed in the eastern side of the Getz-Dotson Trough between February 2010 and December 2016 to measure the CDW inflow to the trough (Figure 1). S1 was deployed at 72.46°S, 116.35°W (local depth ~560 m) on 15 February 2010, 25 December 2011, 2 March 2012, and 3 January 2014 (recoveries and redeployments occurred on the same days). In each respective deployment period, the S1 mooring consisted of five, seven, four, and five MicroCAT Sea-Bird Electronics 37 Serial interface, internal memory, and integral pump (SBE-37SMP) units measuring temperature, conductivity, and pressure, evenly spaced between the bottom and the top buoy at ~320 m depth (with the exception of 2014, during which the top instrument was located at ~260 m). In all years, an upward-looking 150 kHz RD Instruments Workhorse acoustic Doppler current profiler (ADCP) was placed at the bottom measuring current velocity. For each sensor, the data were averaged hourly, and the tides were removed with a 40 hr cutoff Hamming filter.

The MicroCAT and ADCP data were linearly interpolated in the vertical onto a grid with a spacing of 10 m between 300 and 550 m depth, and the gridded data were then monthly averaged. The gridded MicroCAT data were restricted to depths between 330 and 530 m and the ADCP data to the 390–520 m interval, to ensure good data availability in all months. The along-trough velocity was calculated by projecting the velocity components 42° clockwise from the zonal direction to match the orientation of the Getz-Dotson Trough (e.g., Kalén et al., 2016). Conservative temperature (Θ), absolute salinity (SA), and neutral density (γ^n) were computed (Jackett & McDougall, 1997; McDougall & Barker, 2011). In most of 2013, the MicroCATs stopped working, and no data were recorded.

2.2. Ocean Heat Content

Heat content (Q) is calculated from the temperature above the in situ freezing point between 350 and 500 m for mooring S1, according to the following equation:

$$Q = \int_{z1}^{z2} \rho c_p (T - T_0) dz, \tag{1}$$

where $z1 = 500$ m, $z2 = 350$ m, ρ is the in situ ocean density (taken as 1,028 kg m^{-3}), c_p is the specific heat capacity of seawater (taken as 3.99×10^3 J kg^{-1} K^{-1}), T is the in situ temperature, and T_0 is the in situ freezing temperature for each pressure level. Not measuring the surface layers gives comparatively small errors, since the temperature is close to the freezing temperature there (Ha et al., 2014).

2.3. Temperature Decomposition

The partitioning of Θ changes into isopycnal (i.e., changes along isopycnal surfaces; referred to as water mass property changes, WMP) and heave-driven (i.e., vertical displacement of isopycnal surfaces; HVE) components was conducted following Bindoff and McDougall (1994), according to

$$\Delta\Theta|_z \simeq \Delta\Theta|_{\gamma^n} - \Delta z|_{\gamma^n} \overline{\frac{\partial \Theta}{\partial z}}, \tag{2}$$

where $\Delta\Theta$ and Δz represent the temporal deviation from the 2010–2015 time-mean Θ and depth, respectively. $|_z$ and $|_{\gamma^n}$ indicate the evaluation of Θ on depth and γ^n levels, respectively. For the calculation of the right-hand-side terms, Θ values are first binned onto γ^n levels (set to 25.00–28.28 kg m^{-3} every 0.05 kg m^{-3}, refined to 0.01 kg m^{-3} between 26.51 and 27.00 kg m^{-3}, 0.002 kg m^{-3} between 27.002 and 27.70 kg m^{-3}, 0.001 kg m^{-3} between 27.701 and 28.12 kg m^{-3}, and 0.02 kg m^{-3} between 28.14 and 28.28 kg m^{-3}), and vertical gaps are filled by linear interpolation. $\overline{\partial\Theta/\partial z}$ is the 2010–2015 time-averaged vertical gradient of Θ. After each term is calculated, that term is binned back to the grid depth levels, and vertical gaps are linearly interpolated across. The first term on the right-hand side of Equation 2 represents Θ changes on isopycnal levels (WMP). The second term on the right-hand side represents the changes in Θ due to the vertical displacement of isopycnals (HVE). This decomposition is useful to identify the dynamical processes responsible for thermohaline property changes, since each decomposed field is associated with different processes (Bindoff & McDougall, 1994).

2.4. Regional Model Configuration

Monthly-mean outputs of the regional ocean model from Kimura et al. (2017) were employed. Briefly, the simulation uses the Massachusetts Institute of Technology general circulation model (MITgcm) adapted to include sub-ice-shelf cavities (Losch, 2008) and coupled with a sea ice model (Losch et al., 2010). The model domain covers the Amundsen Sea between 75.5°S to 62°S and 80°W to 140°W and includes eight sub-ice-shelf cavities (Getz, Dotson, Crosson, Thwaites, Pine Island, Cosgrove, Abbot, and Venable). The horizontal resolution ranges from 2.8 km in the southern domain to 5.2 km in the northern domain. The model has 50 vertical levels with spacing ranging from 10 m at the surface to 200 m at the bottom. Seabed and ice shelf topography are from the global 1 min Refined Topography data set (Timmermann et al., 2010). Vertical mixing is parameterized with the *K*-profile parameterization (Large et al., 1994). Ocean temperature and salinity initial conditions are from the World Ocean Atlas 2009 (Antonov et al., 2010; Locarnini et al., 2010) interpolated onto the ocean model grid. The atmospheric forcing fields are from ERA-Interim (Dee et al., 2011) applied on the ocean model's surface using the 6-hourly fields (see Kimura et al., 2017). Lateral boundaries are forced with steady climatological fields of temperature, salinity, and velocity from

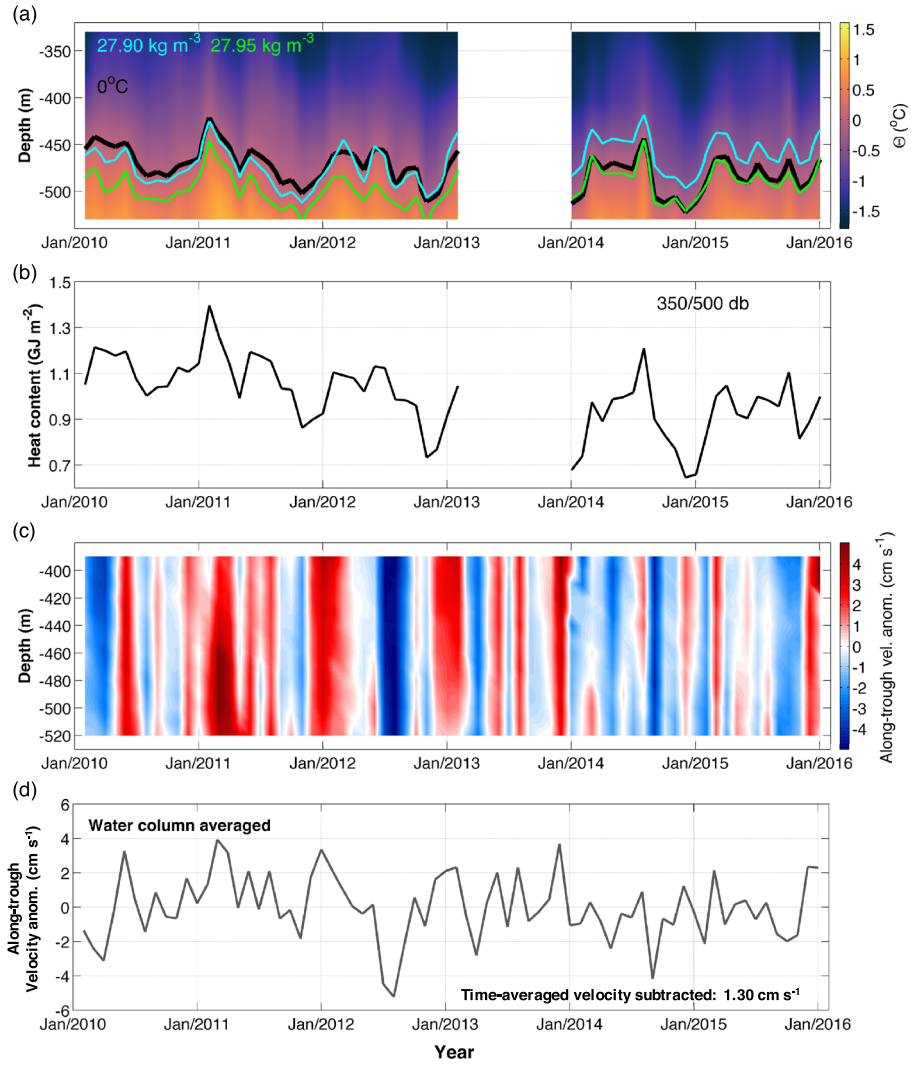

Figure 2. (a) Conservative temperature (Θ) measured by mooring S1. Isotherm of 0°C (black thick line) and γ^n isopycnals of 27.90 (cyan) and 27.95 (green) kg m^{-3} are depicted. Color map from cmocean (Thyng et al., 2016). (b) Monthly heat content (GJ m^{-2}) integrated over 350–500 dbar. (c) Along-trough velocity anomaly (cm s^{-1}) referenced to the 2010–2015 mean velocity profile. Positive (negative) velocity anomaly is directed into (out of) the Getz-Dotson Trough. (d) Water column-averaged velocity anomaly (cm s^{-1}) referenced to the 2010–2015 mean velocity. The time-averaged velocity subtracted from the time series is ~1.3 cm s^{-1}.

a lower-resolution circumpolar model (Holland et al., 2014). The model does not include tidal forcing. The simulation runs from January 1991 to December 2014, and the model was spun up after 1994. More information about the model and the model validation is found in Kimura et al. (2017) and Dotto et al. (2019). For our analyses based on model outputs, potential temperature (θ), practical salinity, and ocean velocity components (zonal, meridional, and vertical), as well as the wind stresses forcing components, over the period of 1995 to 2014 were considered. Heat content was calculated according to Equation 2 over the depth range of 372–522 m for a virtual mooring inserted in the model at the position of mooring S1. Along-trough velocity was also computed for this virtual mooring similarly to the observations.

2.5. Atmospheric Data, Climate Indices, and Sea Surface Height Data

Monthly-mean sea level pressure (SLP) and wind velocity from ERA-Interim (https://www.ecmwf.int/) are considered. From the wind velocity components, the ERA-Interim wind stress is calculated as

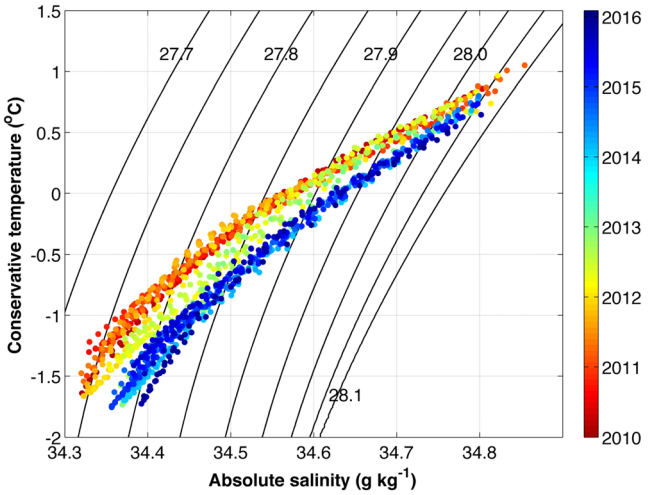

Figure 3. Θ-SA-time diagram for mooring S1 between 2010 and 2016, overlaid by neutral density contours every 0.05 kg m^{-3}.

$$\boldsymbol{\tau} = \rho_a C_d |\boldsymbol{U}| \boldsymbol{U}, \quad (3)$$

where ρ_a is the air density (1.25 kg m^{-3}), C_d is the air-ocean drag coefficient (1.25×10^{-3}), and $\boldsymbol{U}$ is the wind velocity.

The ENSO index is calculated from the sea surface temperature from HadISST1, in the Niño3.4 area averaged over 5°S to 5°N and 170° to 120°W (http://www.esrl.noaa.gov/psd/gcos_wgsp/Timeseries/Nino34/; Rayner et al., 2003). The Southern Annular Mode (SAM) index is from Marshall (2003), obtained from https://legacy.bas.ac.uk/met/gjma/sam.html. The ASL index version 2, which is the area-averaged SLP over the sector 170–298°E and 60–80°S, is from Hosking et al. (2016), found at https://legacy.bas.ac.uk/data/absl/.

Gridded sea level anomaly (SLA) data acquired by CryoSat-2 are used for the period of January 2011 to December 2015. SLA data in ice-covered areas were processed following the method of Peacock and Laxon (2004), which distinguishes between specular echoes from leads and diffuse echoes from sea ice, retrieving measurements in winter. The data set is described in Dotto et al. (2018).

3. Results

CDW was present in the deeper levels of the region during the whole observational period (Figure 2a). A seasonal cycle is present in the Θ measurements. S1 generally exhibits warmer conditions in summer and autumn (February to May) and a colder regime in winter and spring (with coldest conditions in October to November). Similar seasonality is seen for SA (not shown). The MicroCATs distributed over the water column are key to measuring the variability of the thermocline depth, which follows the same seasonality as Θ and SA. The depth of the thermocline is important to the dynamical processes involved in the inflow of CDW onto the shelf (Dotto et al., 2019) and to the interactions of warm waters with the base of the ice shelves (Davis et al., 2018; Jenkins et al., 2016).

From 2010 to 2015, S1 captured a major transition in the Θ field. This entailed a reduction in Θ throughout the water column and a deepening of isotherms (Figure 2a). Along a specific isopycnal (e.g., 27.90 or 27.95 kg m^{-3}), the water cooled by ~0.2°C to ~0.4°C between 2010 and 2015 (Figures 2a and 3). Unfortunately, the MicroCATs did not record data in most of 2013 due to battery issues, thereby losing information about an important part of the transitional period. Nevertheless, a clear change toward cooler and fresher water masses is observed over time in the entire water column (Figure 3). A regime shift is also apparent in the heat content (Figure 2b). During 2010–2013, more heat was potentially available in the trough for ice shelf melting. This period was characterized by a decrease in heat content (from a maximum of ~1.30 GJ m^{-2} in 2011 to a minimum of ~0.70 GJ m^{-2} in 2012). Averaged (±1 standard deviation) heat content was 1.06 ± 0.13 GJ m^{-2} in the period of 2010–2013 and 0.91 ± 0.14 GJ m^{-2} in 2014–2015.

The thermohaline transition of the water masses during 2010–2015 (Figures 2 and 3) can be associated with a different water mass entering the Getz-Dotson Trough or with a vertical displacement of the isopycnals. To quantify the relative importance of each process, we decomposed Θ into changes of water mass properties on isopycnals (i.e., WMP) and changes due to heaving of isopycnals (i.e., HVE), following Equation 2. During 2010–2013, the relatively warmer conditions in the Getz-Dotson Trough were associated with a WMP-induced Θ anomaly (Figures 4a–4d). However, a strong cooling was observed in WMP from mid-2011 to 2013, persisting through 2015 (Figures 4c and 4d). Conversely, the Θ anomaly caused by HVE increased over 2010–2015 (Figures 4b and 4d). Thus, the observed cooling transition captured by the mooring (Figure 4a) was mainly linked to WMP (Figure 4d) and thus involved changes in temperature and salinity that were density compensated. Despite the prevalence of WMP on longer (interannual) time scales in the mooring measurements, Θ changes on shorter periods (i.e., month to month) are mainly due to a vertical displacement of isopycnals (Figure 4d). Consistent with our mooring-based diagnostics, Dotto et al. (2019) found that the period of 2010–2013 was characterized by a dominance of HVE in underpinning the month-to-month variability in the Getz-Dotson Trough in the same regional ocean model that will be

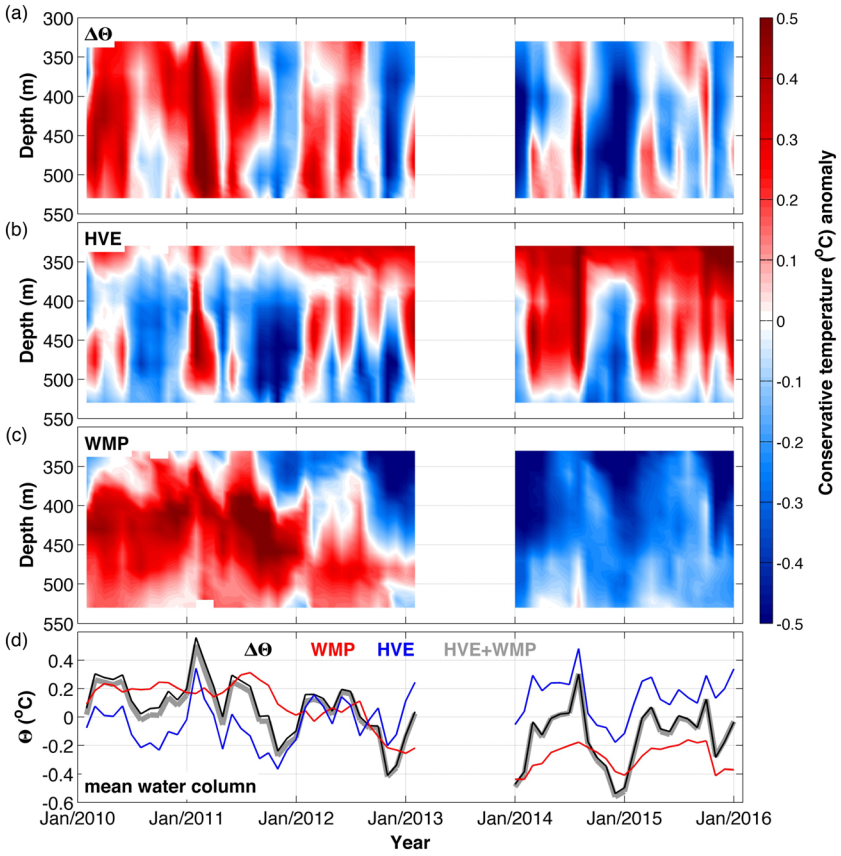

Figure 4. Decomposition of conservative temperature (Θ) for mooring S1. (a) ΔΘ referenced to the 2010–2015 baseline. (b) Change of Θ due to heave (HVE). (c) Change of Θ due to water mass property changes on isopycnals (WMP). (d) Time series of the water column-averaged Θ anomaly for all decomposition terms: ΔΘ (black), reconstructed (gray), HVE (blue), and WMP (red).

evaluated further below. However, on longer time scales, those authors showed that WMP had greater influence on the thermohaline variability in that region.

The S1 bottom-mounted ADCP measured relatively stronger inflow into the Getz-Dotson Trough during the period of elevated heat content (Figures 2c and 2d). Although punctuated by considerable monthly variability (e.g., Wåhlin et al., 2013), there are relatively few inflow events in 2014 and 2015, coinciding with the period of reduced heat content in the trough (Figures 2a and 2b). Mean (±1 standard deviation) along-trough velocity anomaly averaged over the water column was 0.23 ± 2.10 cm s^{-1} in 2010–2013 and -0.46 ± 1.53 cm s^{-1} in 2014–2015 (Figure 2d). Wåhlin et al. (2013) did not observe a clear correlation between inflow velocity in the Getz-Dotson Trough and changes in bottom temperature on short time scales; however, they conjectured that this association could emerge if longer time series were analyzed. Figures 2c and 2d suggest that on seasonal-to-interannual periods, the intensity of the inflowing current is related to the heat content regime in the trough. Since the scarcity of in situ data sets on the shelf break hampers a thorough investigation, we assess the dynamical processes regulating the CDW inflow into the Getz-Dotson Trough with a regional high-resolution sea ice-ocean model in the next section.

4. Discussion

4.1. Oceanic Heat Content Variability in the Getz-Dotson Trough, 2010–2015

The S1 record revealed a transition in water mass properties between 2010 and 2015 (Figures 2 and 3). During this period, waters cooled and freshened along isopycnals (Figure 4), concurrently with a weakening

of bottom-intensified currents at the shelf break that subsequently enter the Getz-Dotson Trough (Figures 1 and 2c). The most pronounced change in water mass properties occurred in 2011–2013 (Figures 2b and 4d).

The interannual variability of the thermohaline properties captured by S1 has been observed by sporadic hydrographic measurements available in different parts of the Amundsen Sea (Dutrieux et al., 2014; Jenkins et al., 2018). The water masses on the continental shelf of the Getz-Dotson Trough experience major shifts in properties on multiannual time scales, which control the heat source for melting the ice shelves downstream, as shown by Jenkins et al. (2018). In front of the Dotson Ice Shelf, these authors documented colder and fresher conditions in 2000, 2014, and 2016 compared to 2011 (in the upper 800 m depth). In contrast, the water mass regime was warmer and saltier in the mid- to end-2000s.

4.2. On-Shelf Heat Content Regulated by Wind Forcing—A Case Study in the Getz-Dotson Trough

In order to determine the dynamics on the wind forcing controlling the heat content of the Getz-Dotson Trough, we now analyze the regional model. The model represents relatively well the water mass structure of the Amundsen Sea, as well as the ocean circulation (Dotto et al., 2019; Kimura et al., 2017). The virtual mooring, taken from the nearest location to mooring S1 in the model, simulates reasonably well the heat content variability in the region, although it is slightly warmer than the observations for the depth ranges selected (Figure 5a). Similarly to the observations, the model shows a decline in the heat content between 2010 and 2014, although this cooling pattern has been simulated since 1995 in the model. The heat content in the model appears to follow a decadal variability, with lower heat content in the early 2000s and mid-2010s, whereas higher heat content is simulated in the mid- to end-2000s, in agreement with observations (Jenkins et al., 2018). The virtual mooring shows higher heat content between May and September, whereas S1 heat content is highest between February and August (Figure 5c). The model broadly reproduces the along-trough velocity variability, mainly in terms of amplitude, in agreement with mooring S1 (Figure 5b). The highest velocities into the trough are observed in end spring to early summer in both data sets, with another peak in June (Figure 5d). The model also shows that the currents crossing the location of mooring S1 are connected to the deep shelf break currents at 372–522 m (Figure 5e). This connection is consistent in most of the Amundsen Sea shelf break, and it is related to the eastward undercurrent (Dotto et al., 2019; Walker et al., 2013).

Next, we examine the role of the wind in driving the currents in the model. Figures 6a and 6b provide spatial maps of the correlation between the along-trough inflow (averaged between depths of 400 and 520 m) measured by mooring S1 and ERA-Interim zonal wind stress (τ_U) and wind stress curl, respectively, for the period of 2011–2015. The time series were deseasonalized and detrended, and temporal gaps in the observations were not filled prior to computing correlations. The maximum correlation values are observed on the continental shelf for τ_U ($r = 0.3$–0.4) and slightly north of the shelf break for wind stress curl ($r = 0.4$–0.5). The analysis was repeated for the model outputs between the along-trough inflow at the location of S1 and τ_U (Figure 6c) and wind stress curl (Figure 6d) for the period of 1995–2014. The observed relationship between shelf break winds and the bottom-intensified currents entering the trough is reproduced by the model and is seen to hold over a longer time period. Positive correlations are found on the continental shelf for τ_U and for the wind stress curl (both showing $r = 0.4$–0.5). Note that the area of high significance level ($p = 0.05$) in the observations is smaller because of the reduced number of effective degrees of freedom compared to the model. The level of correlation ($r \sim 0.4$), however, is similar to that reported in observations for daily time scales (Wåhlin et al., 2013). Thus, it is reasonable to assume that the model is adequately representing the wind-driven dynamics in the Getz-Dotson Trough.

The oceanic circulation in the Amundsen Sea troughs is significantly modulated by wind variability acting on the continental shelf break (Dotto et al., 2019; Kim et al., 2017; Kimura et al., 2017; Thoma et al., 2008; Wåhlin et al., 2013; Webber et al., 2019). The relationships presented in Figure 6 suggest that the bottom-intensified currents measured by mooring S1 should respond (barotropically) to a change in sea surface slope by geostrophy. The change in sea surface slope is determined by the spatial pattern of the wind stress curl, which tends to raise sea level to the north of the shelf break and reduce sea level (or raise it less) to the south of the shelf break. The resulting change in sea level slope then accelerates eastward the undercurrent located at the continental slope. This process is also consistent with Figure 7, which shows the spatial correlation of the SLA and the along-trough velocity measured by mooring S1. The undercurrent follows the bathymetry, and its flow is diverted poleward when it encounters a channel (Klinck, 1996) entering the

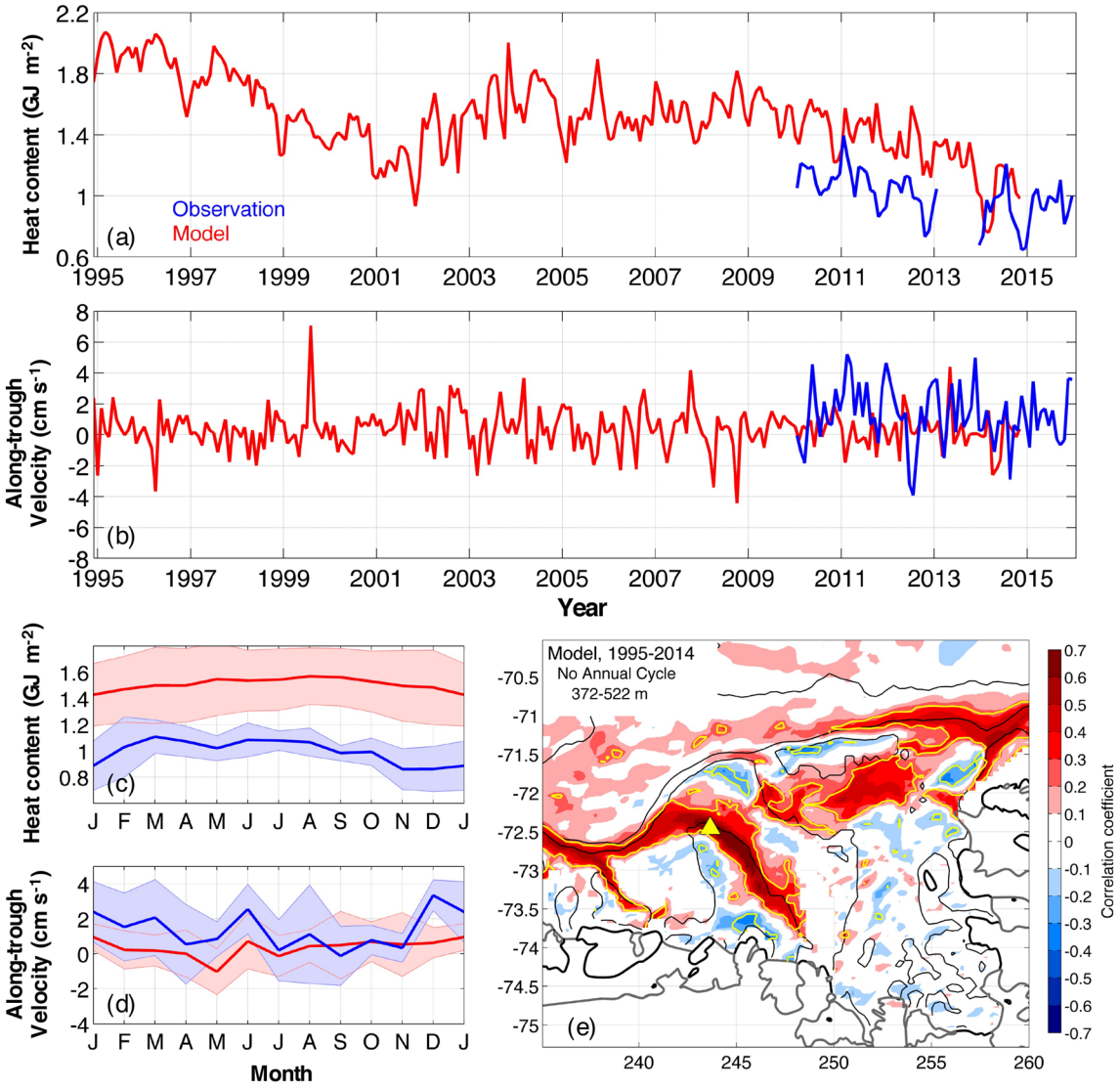

Figure 5. (a) Monthly heat content (GJ m^{-2}) measured by mooring S1 (same as Figure 2b) integrated over 350–500 dbar and in the virtual mooring from the model integrated over 372–522 dbar. (b) Monthly along-trough velocity (cm s^{-1}) measured by mooring S1 and in the virtual mooring from the model, averaged over 390–520 and 372–522 m, respectively. Positive values are southeastward. (c) Annual cycle of the heat content from (a), and (d) annual cycle of the along-trough velocity from (b). Shades in (c) and (d) are the standard deviations for each month. Observations and model are depicted in blue and red, respectively. (e) Correlation between along-trough velocity at the location of mooring S1 averaged over 373–522 m and zonal velocity averaged over 373–522 m at all grid points, between 1995 and 2014. Along-trough velocity is positive southeastward. Yellow triangle indicates the S1 mooring location. Isobaths of 500, 1,000 and 3,000 m are shown (black lines). Trends and annual cycles were removed. *P*-value level of 0.05 is represented by the yellow line.

Getz-Dotson Trough (Figure 5e). Frequently, eastward anomalies in τ_U are associated with an amplification in the strength of the undercurrent velocity along the continental slope of the Amundsen Sea (Dotto et al., 2019) and to an acceleration of the bottom flow into the Getz-Dotson Trough (Wåhlin et al., 2013). It has been suggested that the undercurrent also plays a central role in the oceanic heat delivery to the Pine Island-Thwaites Trough (Figure 1; Assmann et al., 2013; Dotto et al., 2019; Jenkins et al., 2016; Walker et al., 2013; Webber et al., 2019).

Now, we illustrate the hydrographic changes in the Amundsen Sea continental shelf linked to an intensification of the undercurrent (and thus the currents crossing mooring S1; Figure 5e). For this, we select a section along the Getz-Dotson Trough crosscutting the slope (Figure 1), which captures the location where the undercurrent enters the trough (Figure 5e). Composites were created based on periods of intensified (80th percentile) and weakened (20th percentile) undercurrent flow crossing this section (Figure 8). All data

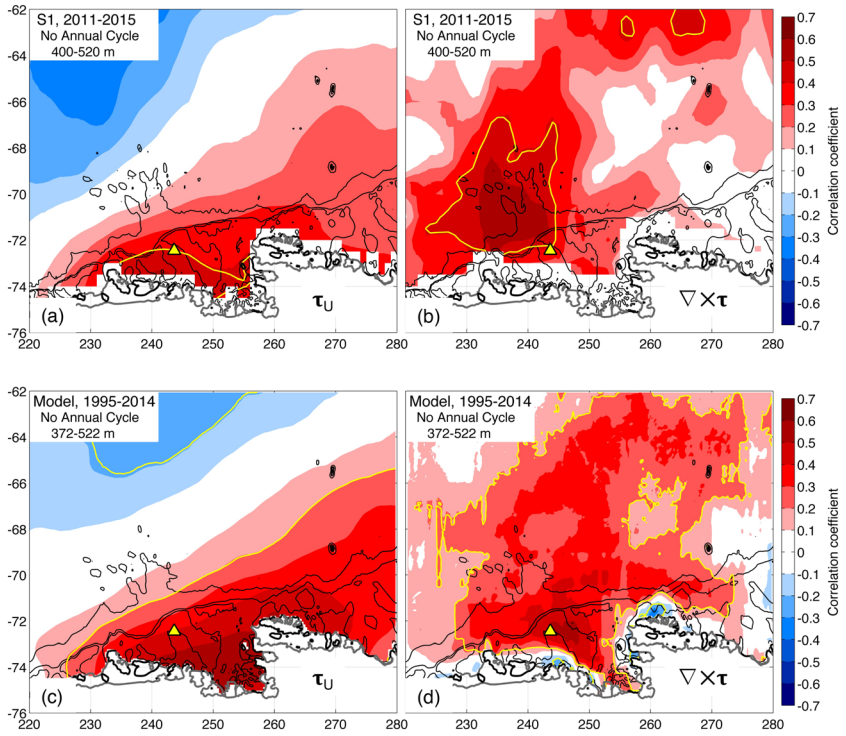

Figure 6. (a) Correlation between S1-measured alo5ng-trough velocity averaged over 400–520 m and ERA-Interim τ_U, for the period 2011–2015. Isobaths of 500, 1,000 and 3,000 m are depicted by black solid lines from IBCSO v1.0 (Arndt et al., 2013). (b) Same as (a), but for the wind stress curl in place of τ_U. (c) Correlation between along-trough velocity at the location of mooring S1 averaged over 373–522 m in the model and the model τ_U for the period 1995–2014. (d) Same as (c), but for the wind stress curl in place of τ_U. Isobaths of 500, 1,000 and 3,000 m are depicted by black solid lines from RTOPO1. Ice shelves are shown in gray. Along-trough velocity is positive southeastward in all cases. Data sets were detrended, and annual cycles were removed. *P*-value level of 0.05 is represented by the yellow line.

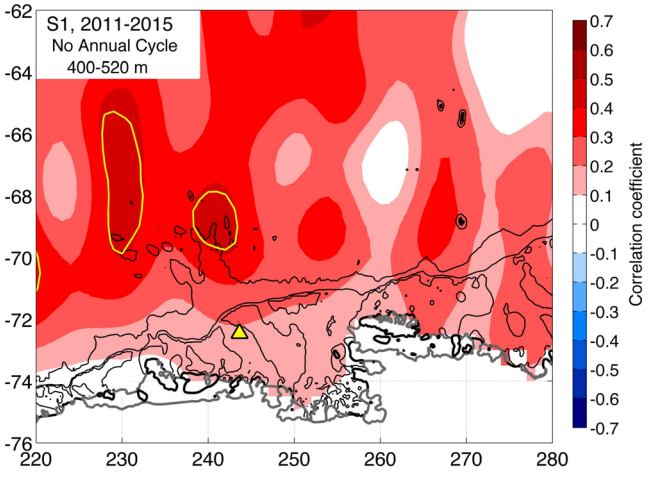

Figure 7. Correlation between S1-measured along-trough velocity averaged over 400–520 m and CryoSat-2 SLA for the period 2011–2015. Along-trough velocity is positive southeastward. Isobaths of 500, 1,000 and 3,000 m are depicted by black solid lines from IBCSO v1.0 (Arndt et al., 2013). Ice shelves are shown in gray. Data sets were detrended, and annual cycles were removed. *P*-value level of 0.05 is represented by the yellow line.

sets were detrended and deseasonalized for this analysis. During strong undercurrent periods, the bottom of the Getz-Dotson Trough is flooded by warmer and saltier waters (Figures 8a and 8b), which are density compensated (not shown). Thus, the inflow of warm waters to the Getz-Dotson Trough is governed by dynamics that primarily affect the WMP component—warming along isopycnals (e.g., Dotto et al., 2019).

Anomalous upwelling is observed all along the slope of the Amundsen Sea, where the undercurrent is active, during the same intensified-undercurrent periods (Figure 8c). Importantly, isopycnals in the proximity of the continental slope are uplifted during these periods (e.g., see the depth of isopycnals $\gamma^n \geq 28.02$ kg m^{-3} near the slope), favoring on-shelf inflow of warmer waters relative to conditions within the trough (Figure 8d). The uplift of isopycnals is arguably associated with a topographic stress acting on the undercurrent (Garrett et al., 1993; Johnson & Killworth, 1975; Lill, 1979), as suggested by, for example, the magnitude of the displacement increasing with depth. Although the model may represent the deepest layers suboptimally due to its low vertical resolution at depth, the relationship documented here is broadly compatible with a bottom Ekman dynamical response to changes in undercurrent intensity, as shown by Wåhlin et al. (2012). When the undercurrent is

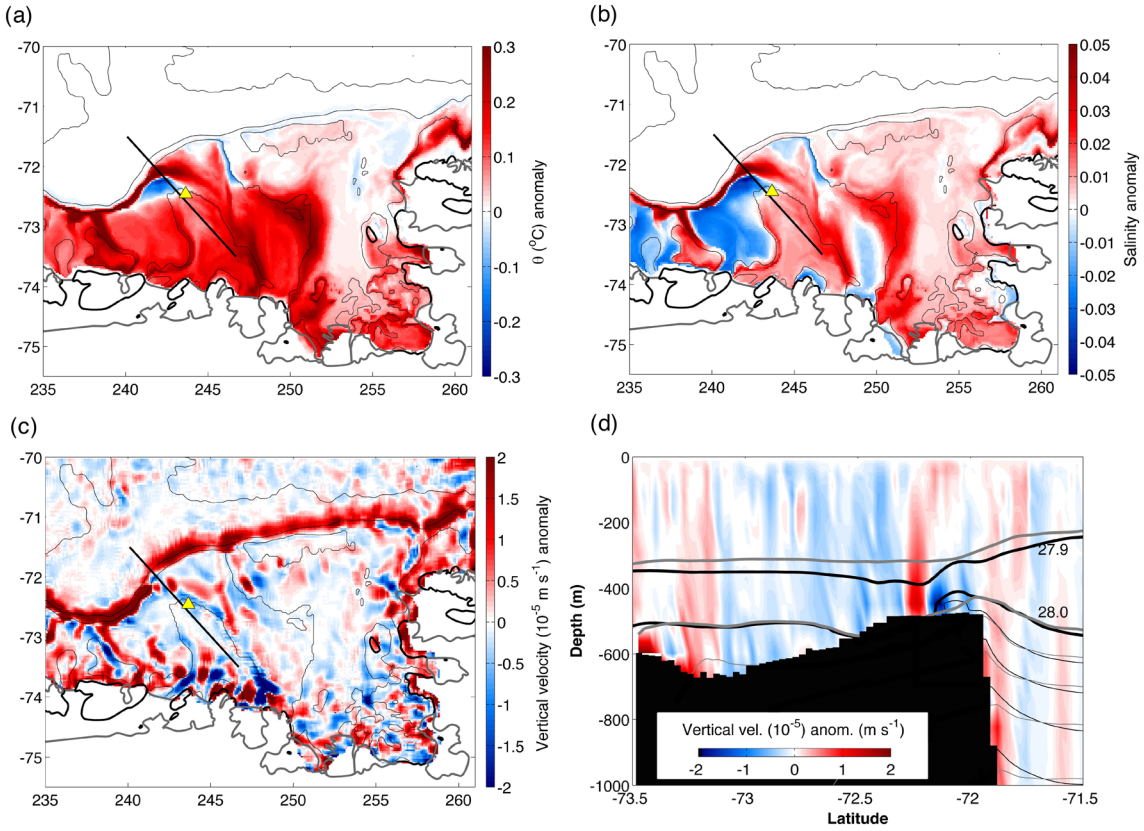

Figure 8. Composites of the bottom properties on the Amundsen Sea continental shelf for periods of intensified undercurrent flow crossing the Dotson section. Anomalies are referenced to the 1995–2014 baseline. Trends and seasonal cycles were removed. (a) θ anomaly, (b) salinity anomaly, and (c) vertical velocity anomaly. Isobaths of 500, 1,000 and 3,000 m are shown (black thin line). Thick black line shows the location of the Dotson section. Yellow triangle depicts the position of mooring S1. Vertical velocity anomaly is smoothed with a boxcar filter of 2 × 2 grid cells. (d) Composite of the vertical velocity anomaly along Dotson section. γ^n surfaces of 27.90 and 28.00 kg m^{-3} are shown by thick lines. Isopycnals for $\gamma^n > 28.00$ kg m^{-3} are spaced every 0.02 kg m^{-3}. Black (gray) contours refer to intensified (weakened) undercurrent periods.

relatively weak, a prevalence of a downwelling anomaly is apparent along the slope (not shown) concurrent with a deepening of isopycnals above the slope (see gray isopycnals in Figure 8d). This configuration hampers the access of warm water onto the continental shelf, resulting in anomalously colder and fresher waters within the trough (not shown).

A latitudinal shift in the zonal wind pattern is observed between periods of strong and weak undercurrent flow (Figure 9). In periods of stronger undercurrent, the wind stress pattern migrates southward, and the 0 N m^{-2} isoline is found near the shelf break (Figure 9a). In addition, the westward winds are weakened on the continental shelf. This shift in the zonal wind sets the condition for an acceleration of the undercurrent at the slope (Dotto et al., 2019) via adjustment to sea level and wind stress curl (Figures 6b, 6d, and 7). Conversely, during weaker undercurrent periods, westward winds are stronger and extend across the continental shelf and shelf break, favoring the deceleration of the currents at the slope (Figure 9b). Considering the association between the circulation within the Getz-Dotson Trough and the shelf break undercurrent (Figure 5e), the along-trough velocity at the site of the S1 mooring is expected to decrease under such wind forcing in both the model and observations. Hence, these results are consistent with the mooring S1 measurements, in the sense that a weaker undercurrent system is associated with cooler conditions within the trough (Figure 2).

4.3. The Effect of the Local Wind on the CDW Core off-Slope

Next, we turn to the question of whether meridional shifts in the CDW core off-slope could influence the inflow of warm waters onto the shelf. For instance, could a wind-induced southward shift of the CDW

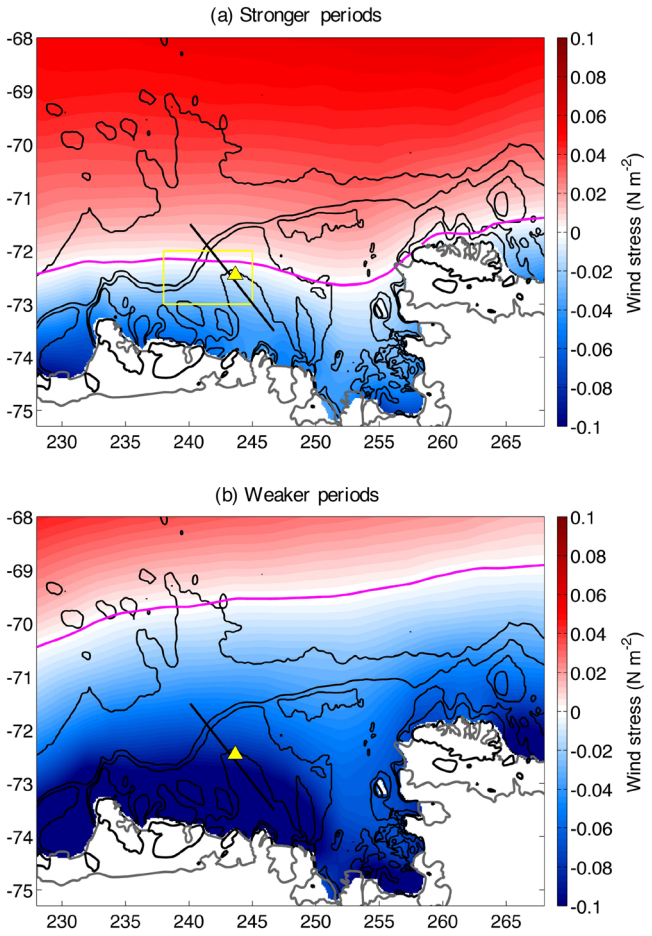

Figure 9. Same as Figure 8, but for the model τ_U for periods of a strong and b weak undercurrent flow crossing the Dotson section. The zero zonal wind stress isoline is shown in magenta. Trends and seasonal cycles were removed. The yellow rectangle in (a) shows the area used to extract the time series of the τ_U for Figure 10.

core lead to warmer conditions in the Getz-Dotson Trough during the period analyzed? To examine this issue, composites were constructed for periods of maximum τ_U, that is, anomalous eastward wind leading to a warming of the Getz-Dotson Trough, and minimum τ_U, that is, anomalous westward wind leading to a cooling of the Getz-Dotson Trough. The thresholds were, respectively, the 80th and 20th percentiles. The time series of the τ_U anomaly was selected at the shelf break as the monthly-mean value over 72–73°S and 238–245°E (Figure 9a), identified as the area of strongest coupling between eastward wind forcing and bottom speed (Dotto et al., 2019). The time integral of the τ_U anomaly over January 1995 to December 2014 is used (Figure 10a), following Dutrieux et al. (2014) and Jenkins et al. (2016). The stronger and longer-lasting the eastward winds are, the more enhanced and sustained flooding of warmer water to the Getz-Dotson Trough is expected to be. Figure 10a shows that the periods of intense and weak time integral of τ_U broadly follow the warm and cold years reported by Jenkins et al. (2018).

While the expected difference in θ in the Getz-Dotson Trough between the two periods is observed (Figures 10b and 10c), no appreciable difference in the location and shape of the CDW core (take the isotherm 1.5°C for reference) is identified. Rather, the southern location of the CDW core at the shelf break (~72°S) is essentially unchanged between both periods. This suggests that meridional shifts in the CDW off-slope do not exert a significant influence on the on-shelf heat content of the Getz-Dotson Trough over the period analyzed. Therefore, variations in local winds governing the undercurrent dynamics (Figures 6 and 8) are more important than the location of CDW offshore in regulating the access of warm waters to the Getz-Dotson Trough via uplifting of the isopycnals over the continental slope on the time scales considered here (Figure 10c). A caveat of this analysis is that the model is forced with climatological boundary conditions and may not represent long-term changes in the position of the Antarctic Circumpolar Current. On longer time scales (e.g., decades and longer), it is possible that variations in the large-scale winds may lead to changes in the water masses carried by the Antarctic Circumpolar Current, which could affect the margins of West Antarctica (Nakayama et al., 2018). A potential role for remote winds in shaping the on-shelf heat content of the Amundsen Sea via propagation of coastal-trapped waves has also been highlighted (e.g., Spence et al., 2017; Webb et al., 2019).

To summarize, the mechanism documented here entails the modulation by local winds of the along-slope undercurrent's intensity and the associated uplifting of isopycnals over the continental slope, which determines the extent to which warm waters flood the Getz-Dotson Trough (Figures 5–10). Anomalous eastward shelf break winds increase the sea level offshore (and reduce it onshore), inducing a strengthening of the slope undercurrent (Figure 11). A stronger undercurrent leads to an uplift of the isopycnals at the slope by bottom Ekman dynamics. When these isopycnals trespass the shelf break, CDW enters the Getz-Dotson Trough (Figure 11). Associated to that, the bottom-intensified currents at S1 are also strengthened (Figure 5e). The more pronounced and sustained an eastward shelf break wind anomaly is, the more favorable the conditions are for a warming on the continental shelf because heat content responds gradually and cumulatively to changes in winds/undercurrent strength (Figures 8, 10, and 11). In turn, a westward shelf break wind anomaly is associated with a cooling on the continental shelf. This relationship does not involve meridional shifts of the CDW core off-slope (Figure 10b).

The warming of the Antarctic continental shelf by a southward shift of the zonal winds induced by greenhouse gas emission was discussed by Spence et al. (2014). In their work, the shoaling of the isopycnals was set by the weakening of the Ekman pumping near the coast. The mechanism we propose here is

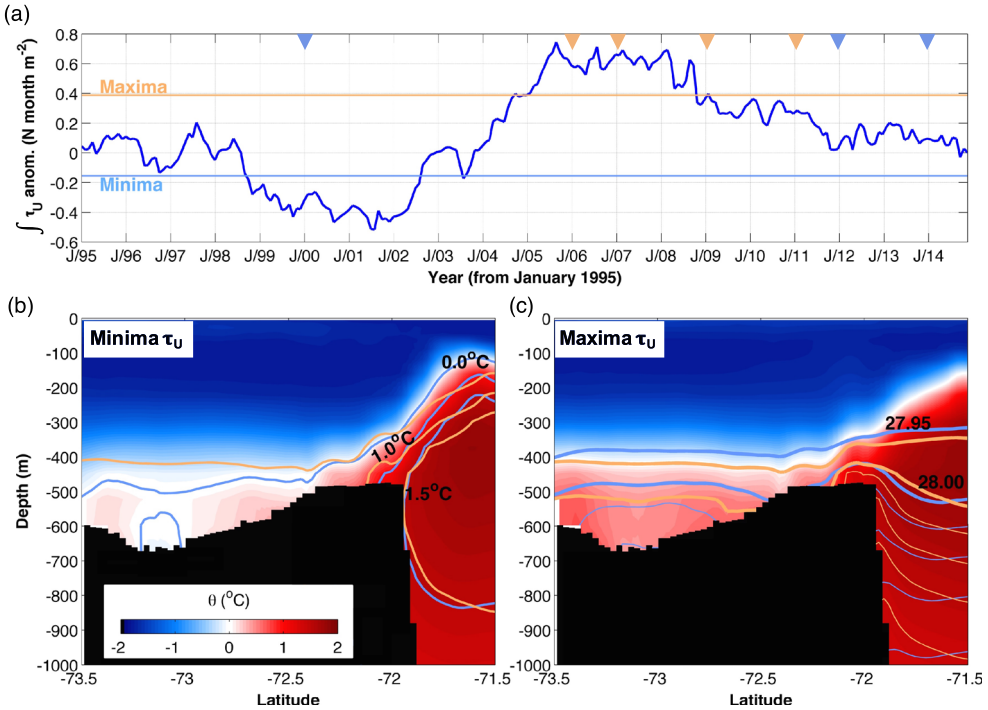

Figure 10. (a) Time integral of the modeled shelf break τ_U anomaly for the interval between January 1995 and December 2014, from the area highlighted by the yellow rectangle in Figure 8. Solid lines indicate the periods of maximum (80th percentile; orange) and minimum (20th percentile; light blue) time-integrated τ_U. Inversed triangles depict warm (orange) and cold (light blue) years according to Jenkins et al. (2018). (b) Composite of θ in the Dotson section (Figure 1 for section location) for the minimum time-integrated τ_U periods. Orange (light blue) lines represent the isotherms of 0.0°C, 1.0°C, and 1.5°C for maximum (minimum) time-integrated τ_U anomaly periods. (c) Composite of θ in the Dotson section for the maximum time-integrated τ_U anomaly periods. Orange (light blue) lines represent the isopycnals of 27.95 and 28.00 kg m^{-3} for maximum (minimum) time-integrated τ_U anomaly periods. $\gamma^n > 28.00$ kg m^{-3} surfaces (thin lines) are spaced every 0.02 kg m^{-3}.

strengthened by the undercurrent, which is driven by the shelf break wind/wind stress curl and sets the uplift of the isopycnals near the slope (Figure 11).

4.4. Drivers of Zonal Wind Perturbations at the Shelf Break of the Getz-Dotson Trough

The time series of ERA-Interim shelf break τ_U is extracted over the same area, 72–73°S and 238–245°E (Figure 9a). Then, the time integral of the monthly-mean τ_U anomaly over the interval of January 1980 to March 2016 is calculated. Figure 12a shows that there is a close relationship between the time-integrated τ_U and the on-shelf heat content measured by mooring S1 and the virtual mooring from the model simulation. This suggests that a prevalence of anomalously westward τ_U is associated with a decrease in the heat content observed within the trough. The period of 2011–2012, which exhibited a rapid decline in mooring-measured heat content, also exhibits a prominent reduction in the time-integrated τ_U (Figure 12a). After 2013, the time-integrated τ_U and the heat content are reduced. Note that earlier periods documented as cool regimes in the Amundsen Sea (e.g., early 2000s; Jenkins et al., 2018) coincide with times of low-to-negative time-integrated τ_U anomaly, that is, a prevalence of weak eastward or westward wind. In turn, periods with warmer conditions (e.g., mid- to end-2000s; Jenkins et al., 2018) coincide with positive time-integrated τ_U, that is, stronger eastward wind. Thus, the variations in the local winds match the decadal oceanic regime transitions discussed by Jenkins et al. (2018). But what drives these changes in the local winds?

The wind variability in the Amundsen Sea is primarily associated with shifts in the strength and location of the ASL system centered in the Amundsen-Bellingshausen Seas (Hosking et al., 2013, 2016; Raphael et al., 2016; Turner et al., 2013). Assuming no shift in the position of the ASL, a negative SLP anomaly

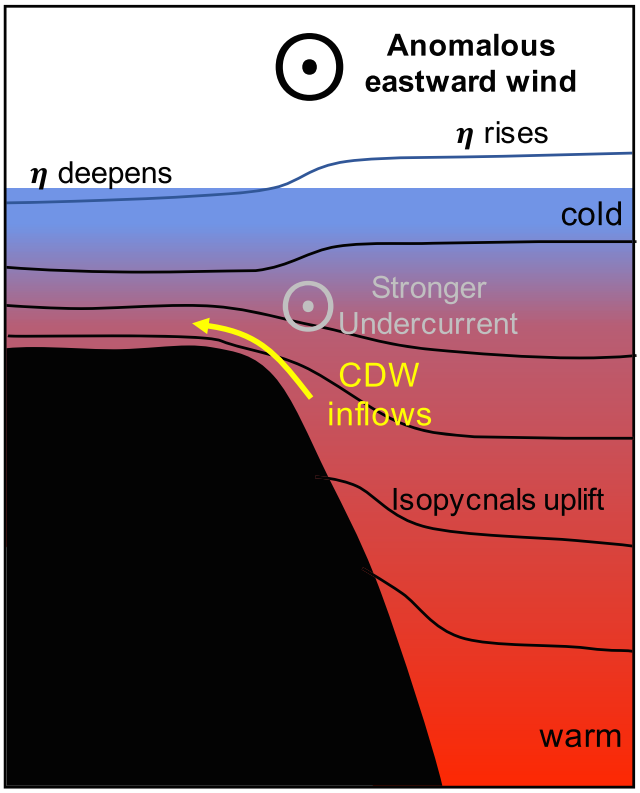

Figure 11. Schematic of the CDW inflow in the Getz-Dotson Trough. Anomalous eastward winds induce an increase of seal level (η) off-slope and a decrease in η near the coast. This change in the meridional gradient of η leads to a strengthening of the eastward undercurrent. The undercurrent leads to an uplift of the isopycnals near the slope, which brings CDW up-slope until it crosses the shelf break and enters the Getz-Dotson Trough. With an anomalous westward wind, the opposite is seen. η deepens (rises) offshore (near the coast), which induces a weakening of the undercurrent. The isopycnals near the slope deepen, and the access of CDW into the Getz-Dotson Trough is reduced.

should increase the westward wind at the shelf break, whereas a positive SLP anomaly would decrease the westward wind intensity, by modulating the atmospheric cyclonic circulation associated with the low-pressure system. Further, latitudinal changes in the central position of the ASL may affect the intensity of the shelf break wind in the sense that the cyclonic wind around the low-pressure system moves inland or offshore according to the latitude of the center of the ASL. Thus, if the low-pressure system moves northward, there might be an increase in westward wind anomalies near the continental slope. If the low-pressure system moves southward, there might be an increase in eastward wind anomalies near the continental slope.

To assess the effect of the ASL on the local τ_U, the time integrals of the anomaly of the ASL index and of the τ_U anomaly were calculated over January 1980 to March 2016. Figure 12b indicates the existence of a close relationship between the time-integrated ASL and the time-integrated τ_U ($r = 0.84$, $p < 0.01$). Anomalously low ASL pressure leads to a stronger westward wind anomaly at the shelf break, whereas anomalously high ASL pressure leads to a stronger eastward wind anomaly at the shelf break (Figures 12a and 12b). The time-integrated effect of the latitude or longitude of the ASL does not exhibit a relationship with the local time-integrated τ_U (not shown).

The ASL variations in intensity and location are related to ENSO and SAM (Clem et al., 2017; Fogt et al., 2011; Lachlan-Cope & Connolley, 2006; Raphael et al., 2016; Turner et al., 2017). The time integrals of ENSO and SAM indices over January 1980 to March 2016 are significantly correlated with the time integral of the anomaly of the ASL index ($r = 0.75$ and $r = -0.64$, respectively, both significant at the 95% level). When El Niño and a negative phase of SAM occur concurrently, the regional SLP anomaly associated with the ASL increases, resulting in an eastward wind anomaly at the Amundsen Sea shelf break (Clem et al., 2017; Turner et al., 2013, 2017). The opposite anomalies emerge in association with concurrent La Niña and positive SAM states, leading to lower regional SLP associated with the ASL and a westward wind anomaly at the shelf break. However, the effects of ENSO and SAM on the ASL may be subdued when the two climatic modes are in opposite phases (Fogt & Bromwich, 2006). Previous studies have attempted to explain the relation of wind forcing with oceanic heat delivery onto the Amundsen Sea continental shelf in terms of large-scale climatic modes (e.g., Dutrieux et al., 2014; Holland et al., 2019; Jenkins et al., 2016; Steig et al., 2012). The time-integrated shelf break τ_U is most closely related to the time-integrated ASL index ($r = 0.84$, $p < 0.01$), followed by the time-integrated ENSO index ($r = 0.65$, $p < 0.01$). No significant correlation is found between the time-integrated shelf break τ_U and the time-integrated SAM index. Thus, the ASL, which is influenced by SAM and ENSO, is identified as the key regulator of the shelf break τ_U that drives transitions between warm and cold conditions in the Getz-Dotson Trough.

In order to provide a synthesis of the atmospheric state characteristically associated with the prevalence of anomalously westward/eastward zonal wind forcing at the Getz-Dotson Trough shelf break, composites of SLP anomaly and wind component anomalies are constructed. During anomalously westward shelf break τ_U (Figure 12a), the mean regional SLP is anomalously negative, reflecting a deeper ASL (Figure 13a). In this case, the mean wind pattern at the shelf break is anomalously westward, which is associated to a weakening of the along-slope undercurrent, a deepening of isopycnals over the slope, and reduced inflow of warm waters onto the shelf. This results in less heat entering the Getz-Dotson Trough. In contrast, during anomalously eastward shelf break τ_U (Figure 12a), the mean regional SLP is anomalously positive (Figure 13b). Consequently, this results in a mean eastward wind anomaly at the shelf break, which is associated to an intensification of the undercurrent, uplifting of isopycnals over the slope, and readier access of warmer

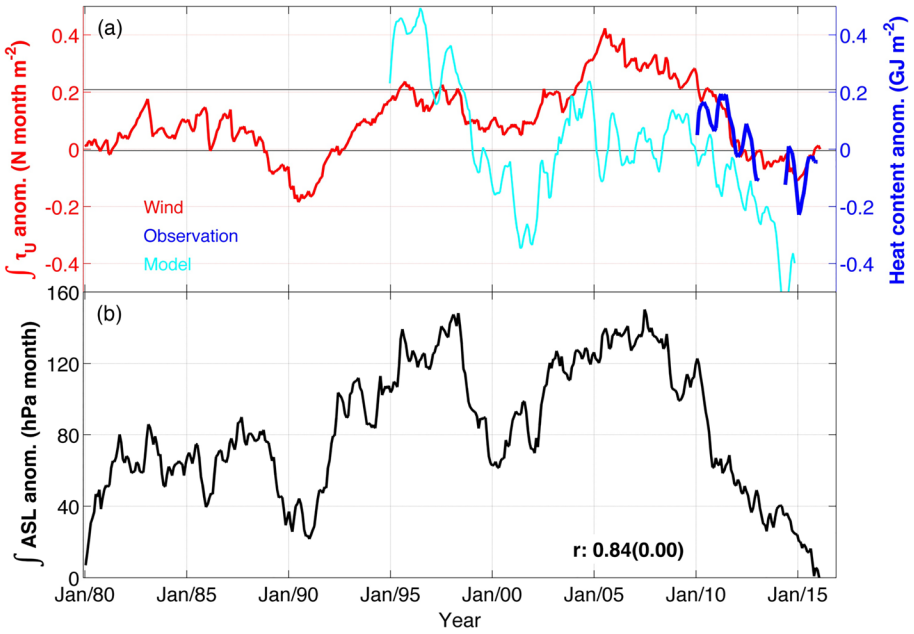

Figure 12. (a) Time integral of the ERA-Interim shelf break τ_U anomaly over the interval of January 1980 to March 2016 (red; extracted from the area highlighted in Figure 9a) and the S1-measured (blue) and model-simulated (cyan) heat content anomaly smoothed with a 6-month running mean filter. Black lines depict the 20th and 80th percentiles of the time-integrated shelf break τ_U anomaly. (b) Time integral of the ASL index anomaly for the interval between January 1980 and March 2016. Correlation coefficient and *p*-value (in brackets) between the time-integrated ASL and the time-integrated τ_U are shown.

waters onto the Getz-Dotson Trough (Figures 10 and 11). Taking the 980 hPa to track the ASL location, no apparent shift of the low-pressure central position is noted between the two contrasting scenarios; the low SLP center (980 hPa) is located at ~72.5°S and ~145°W in both cases.

In summary, the evidence presented in this work suggests that the ASL regulates the oceanic heat content in the Getz-Dotson Trough by controlling zonal winds at the Amundsen Sea shelf break (Figure 12). Then, this τ_U, through the wind stress curl, governs the undercurrent's intensity (Figures 6b and 6d), which regulates the shelf break isopycnal depths and the rate of on-shelf access of the warm waters, providing the heat source for melting the regional ice shelves. A prevalence of periods with anomalously negative ASL state results in a reduction in the heat content of the Getz-Dotson Trough.

4.5. The ASL's Seasonal Control of the Heat Content of the Getz-Dotson Trough

The ASL has a strong seasonal cycle in terms of pressure and location (Hosking et al., 2016). Figure 14 shows the sequence of the annual cycle of the SLP over 1980–2015 for our study region. In summer, the ASL is less deep and is located northeastward (toward the Bellingshausen Sea). In spring, the SLP of the ASL drops, and its position moves southwestward (toward the Ross Sea).

The changes in pressure and position of the ASL are relatively rapid, and the ocean may not adjust to the atmospheric forcing on month-to-month time scales. However, when a longer sequence of change in SLP is analyzed (i.e., its time integral), we start to see a pattern associated with the seasonality of the heat content (Figure 5c). For instance, the strong low-pressure system that prevails from August to November generates (by geostrophy) westward winds along the shelf break of the Getz-Dotson Trough (Figure 14). During this period, heat content decreases in association with weaker along-trough velocity at S1 (Figures 5c and 5d).

In summer, the isobars are not oriented along the coast, and the along-trough velocity accelerates (Figure 5d). It is likely that the slope undercurrent is stronger in this season (by its correlation with the trough currents shown in Figure 5e) and may uplift the isopycnals at the shelf break, which then allows warm waters to enter the Getz-Dotson Trough (Figure 11). During January to March, the heat content within the trough slowly increases, reaching its maximum in March (Figure 5c). Then, when the ASL

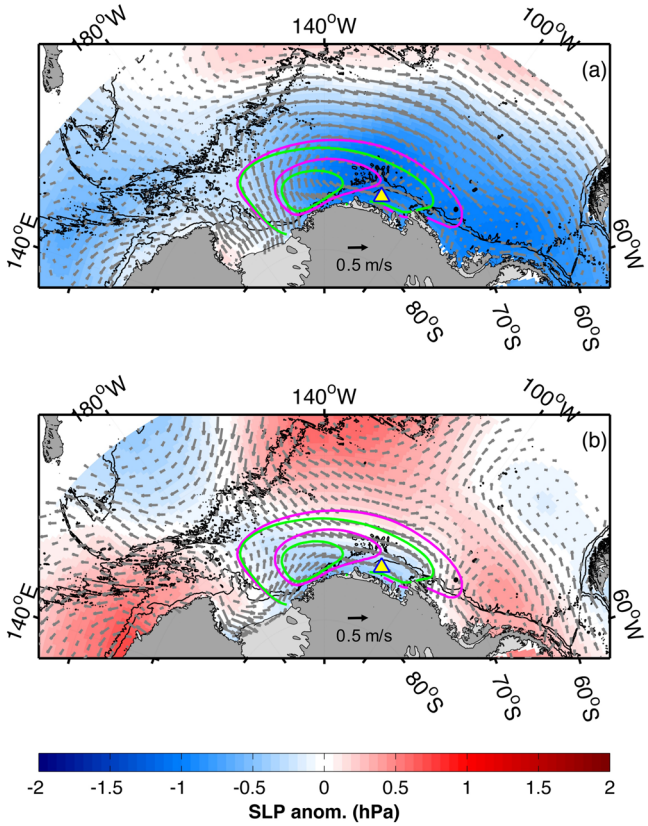

Figure 13. Composites of SLP anomaly and wind stress anomaly for the strong and weak periods of the time-integrated shelf break zonal wind stress anomaly. (a) ERA-Interim SLP anomaly and wind stress anomaly averaged for times when the time-integrated zonal wind stress anomaly in Figure 12a is weak (20th percentile). (b) Same as (a), but for times when the time-integrated zonal wind stress anomaly is strong (80th percentile). Isobaths of 1,000 and 3,000 m are depicted. Yellow triangle shows the location of mooring S1. Values of 980 and 982 hPa for strong (green) and weak (magenta) wind periods, respectively, indicate the mean location of the ASL for both scenarios.

migrates southwestward, the isobars are again aligned with the coast, leading to wind conditions that decrease the bottom-intensified current at S1 (Figure 5d) and thereby to a gradual decrease in the heat content until May. In June (with the small increase in SLP), the currents intensify and create conditions for a new increase in heat content (Figures 5c and 5d). After June, the currents weaken, and the heat content gradually decreases again.

Conclusions

In this work, we have shown that the oceanic heat content measured by a multiyear mooring located in a major trough of the Amundsen Sea continental shelf (the Getz-Dotson Trough) decreased in association with a weakening of the CDW inflow over 2010–2015 (Figure 2). The trough inflow is connected to the onshore extension of an along-slope undercurrent (Figure 5e). The intensity of the undercurrent is regulated by zonal wind stress (and its curl) at the shelf break (Figure 6) and is coupled to an uplifting of isopycnals above the slope that enables access of CDW to the trough (Figures 10 and 11). Westward anomalies of the wind stress at the shelf break are associated with a deeper ASL (Figure 12). The ASL exerts an important control on the undercurrent-mediated inflow of warm waters onto the Amundsen Sea continental shelf. A deeper ASL is responsible for colder anomalies in the Getz-Dotson Trough and for an intensification of the westward coastal flow (via enhancement of surface convergence and sea level at the Antarctic coast; e.g., Dotto et al., 2018), which may export meltwater from Dotson and Getz Ice Shelves via coastal jets (Nakayama et al., 2014).

Although Thompson et al. (2018) define a transition between warm shelf and fresh shelf approximately at the Getz-Dotson Trough, the role of the ASL in controlling the heat content variability may be widely relevant across the Amundsen Sea troughs. This is suggested by the facts that (i) both the Getz-Dotson Trough and the troughs to the east warm and cool concurrently (e.g., Dotto et al., 2019; Dutrieux et al., 2014; Jacobs et al., 2011; Jenkins et al., 2018) and (ii) the undercurrent varies as a coherent feature along the slope of both sides of the Amundsen Sea (Assmann et al., 2013; Dotto et al., 2019; Walker et al., 2013), thereby indicating that the ASL might also control heat content in the Pine Island-Thwaites Trough using a mechanism similar to those described here. However, corroborating the relationship of the ASL with the heat content variability in the Pine Island-Thwaites Trough is a task for future work.

Although we have not identified meridional shifts of the ASL as being important on the time scales considered by this study (Figure 13), climate model simulations have suggested that a poleward and eastward migration of the low-pressure system will unfold during the remainder of this century (Hosking et al., 2016) in association with the southward migration of the westerlies (Holland et al., 2019). This configuration is likely to lead to stronger eastward winds at the shelf break of the Amundsen Sea as the cyclonic circulation associated with the ASL migrates southward. Hence, an enhancement of warm ocean anomalies in the Amundsen Sea troughs is to be expected (Holland et al., 2019).

Data Availability Statement

The mooring data are available online (at https://data.nodc.noaa.gov/cgi-bin/iso?id=gov.noaa.nodc:0211128) or from AW (anna.wahlin@marine.gu.se). The MITgcm model code is found in http://mitgcm.org, and the model output data used in the current work are available online (at http://doi.org/10.5281/zenodo.3937466) or from S. K. (skimura@jamstec.go.jp). SLA data can be accessed via http://

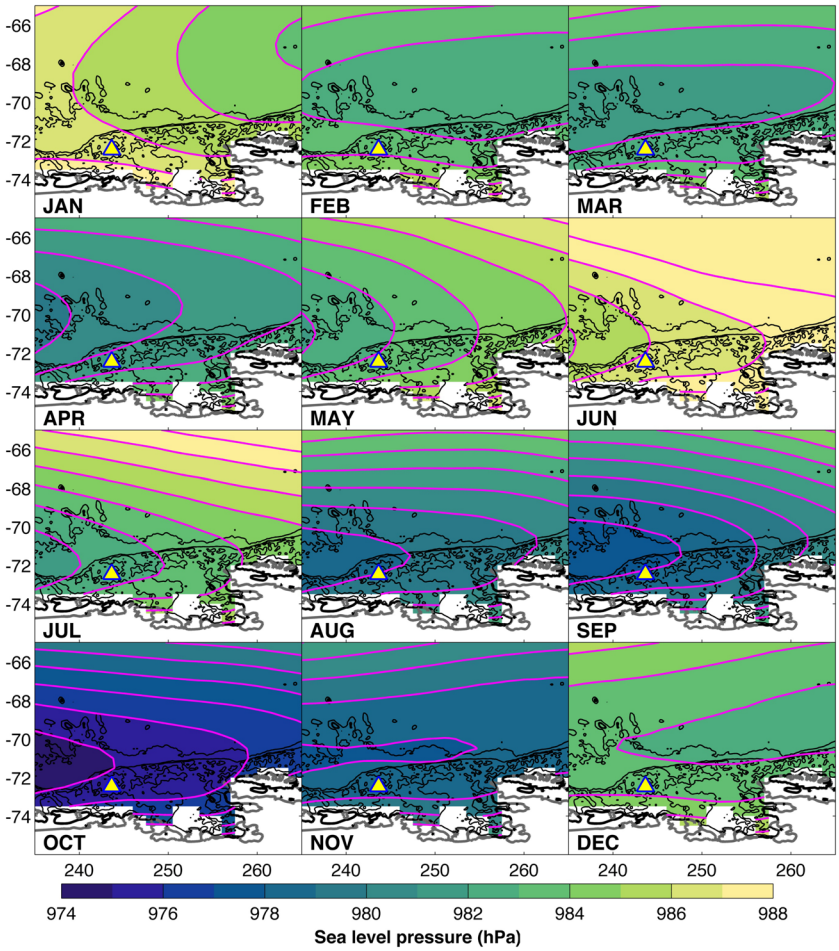

Figure 14. Annual cycle of ERA-Interim SLP in the Amundsen Sea over 1980–2015. Magenta contours depict isobars, and the yellow triangle shows the location of mooring S1 in the Getz-Dotson Trough. Isobaths of 500, 1,000 and 3,000 m are indicated by black solid lines from IBCSO v1.0 (Arndt et al., 2013). Color map is from cmocean (Thyng et al., 2016).

www.cpom.ucl.ac.uk/dynamic_topography_west_antarctica/ or from TSD (tiagosdotto@gmail.com). ERA-Interim, ENSO, SAM, and ASL indices were cited along the manuscript.

Acknowledgments

T. S. D. acknowledges support by the CNPq-Brazil PhD scholarship (232792/2014-3) and CNPq-Brazil PDJ scholarship (151248/2019-2). A. C. N. G. was supported by the Royal Society and the Wolfson Foundation. M. T. acknowledges support from the SKIM Mission Science Study Project "SKIM-SciSoc" (ESA-RFP 3-15456/18/NL/CT/gp) and the ESA "CryoSat+ Antarctica Ocean" project (ESA AO/1-9156/17/I-BG).

References

Antonov, J. I., Seidov, D., Boyer, T. P., Locarnini, R. A., Mishonov, A. V., Garcia, H. E., et al. (2010). World ocean atlas 2009, volume 2: Salinity. In S. Levitus (Ed.), *NOAA Atlas NESDIS 69* (p. 184). Washington, DC: U.S. Government Printing Office.

Arndt, J. E., Schenke, H. W., Jakobsson, M., Nitsche, F. O., Buys, G., Goleby, B., et al. (2013). The International Bathymetric Chart of the Southern Ocean (IBCSO) Version 1.0—A new bathymetric compilation covering circum-Antarctic waters. *Geophysical Research Letters*, *40*, 3111–3117. https://doi.org/10.1002/grl.50413

Assmann, K. M., Darelius, E., Wåhlin, A. K., Kim, T. W., & Lee, S. H. (2019). Warm Circumpolar Deep Water at the western Getz Ice Shelf front, Antarctica. *Geophysical Research Letters*, *46*, 870–878. https://doi.org/10.1029/2018GL081354

Assmann, K. M., Jenkins, A., Shoosmith, D. R., Walker, D. P., Jacobs, S. S., & Nicholls, K. W. (2013). Variability of Circumpolar Deep Water transport onto the Amundsen Sea continental shelf through a shelf break trough. *Journal of Geophysical Research: Oceans*, *118*, 6603–6620. https://doi.org/10.1002/2013JC008871

Bindoff, N. L., & McDougall, T. J. (1994). Diagnosing climate change and ocean ventilation using hydrographic data. *Journal of Physical Oceanography*, *24*(6), 1137–1152. https://doi.org/10.1175/1520-0485(1994)024<1137:DCCAOV>2.0.CO;2

Chavanne, C. P., Heywood, K. J., Nicholls, K. W., & Fer, I. (2010). Observations of the Antarctic Slope Undercurrent in the southeastern Weddell Sea. *Geophysical Research Letters*, *37*, L13601. https://doi.org/10.1029/2010GL043603

Christianson, K., Bushuk, M., Dutrieux, P., Parizek, B. R., Joughin, I. R., Alley, R. B., et al. (2016). Sensitivity of Pine Island Glacier to observed ocean forcing. *Geophysical Research Letters*, *43*, 10,817–10,825. https://doi.org/10.1002/2016GL070500

Clem, K. R., Renwick, J. A., & McGregor, J. (2017). Large-scale forcing of the Amundsen Sea Low and its influence on sea ice and West Antarctic temperature. *Journal of Climate*, *30*(20), 8405–8424. https://doi.org/10.1175/JCLI-D-16-0891.1

Davis, P. E. D., Jenkins, A., Nicholls, K. W., Brennan, P. V., Abrahamsen, E. P., Heywood, K. J., et al. (2018). Variability in basal melting beneath Pine Island Ice Shelf on weekly to monthly timescales. *Journal of Geophysical Research: Oceans*, *123*, 8655–8669. https://doi.org/10.1029/2018JC014464

Dee, D. P., Uppala, S. M., Simmons, A. J., Berrisford, P., Poli, P., Kobayashi, S., et al. (2011). The ERA-interim reanalysis: Configuration and performance of the data assimilation system. *Quarterly Journal of the Royal Meteorological Society*, *137*(656), 553–597. https://doi.org/10.1002/qj.828

Dotto, T. S., Naveira Garabato, A., Bacon, S., Tsamados, M., Holland, P. R., Hooley, J., et al. (2018). Variability of the Ross Gyre, Southern Ocean: Drivers and responses revealed by satellite altimetry. *Geophysical Research Letters*, *45*, 6195–6204. https://doi.org/10.1029/2018GL078607

Dotto, T. S., Naveira Garabato, A. C., Bacon, S., Holland, P. R., Kimura, S., Firing, Y. L., et al. (2019). Wind-driven processes controlling oceanic heat delivery to the Amundsen Sea, Antarctica. *Journal of Physical Oceanography*, *49*(11), 2829–2849. https://doi.org/10.1175/JPO-D-19-0064.1

Dutrieux, P., De Rydt, J., Jenkins, A., Holland, P. R., Ha, H. K., Lee, S. H., et al. (2014). Strong sensitivity of Pine Island ice-shelf melting to climatic variability. *Science*, *343*(6167), 174–178. https://doi.org/10.1126/science.1244341

Fogt, R. L., & Bromwich, D. H. (2006). Decadal variability of the ENSO Teleconnection to the high-latitude South Pacific governed by coupling with the Southern Annular Mode. *Journal of Climate*, *19*(6), 979–997. https://doi.org/10.1175/JCLI3671.1

Fogt, R. L., Bromwich, D. H., & Hines, K. M. (2011). Understanding the SAM influence on the South Pacific ENSO teleconnection. *Climate Dynamics*, *36*(7-8), 1555–1576. https://doi.org/10.1007/s00382-010-0905-0

Garrett, C., MacCready, P., & Rhines, P. (1993). Boundary mixing and arrested Ekman layers: Rotating stratified flow near a sloping boundary. *Annual Review of Fluid Mechanics*, *25*(1), 291–323. https://doi.org/10.1146/annurev.fl.25.010193.001451

Ha, H. K., Wåhlin, A. K., Kim, T. W., Lee, S. H., Lee, J. H., Lee, H. J., et al. (2014). Circulation and modification of warm deep water on the central Amundsen Shelf. *Journal of Physical Oceanography*, *44*(5), 1493–1501. https://doi.org/10.1175/JPO-D-13-0240.1

Holland, P. R., Bracegirdle, T. J., Dutrieux, P., Jenkins, A., & Steig, E. J. (2019). West Antarctic ice loss influenced by internal climate variability and anthropogenic forcing. *Nature Geoscience*, *12*(9), 718–724. https://doi.org/10.1038/s41561-019-0420-9

Holland, P. R., Bruneau, N., Enright, C., Losch, M., Kurtz, N. T., & Kwok, R. (2014). Modeled trends in Antarctic Sea ice thickness. *Journal of Climate*, *27*(10), 3784–3801. https://doi.org/10.1175/JCLI-D-13-00301.1

Hosking, J. S., Orr, A., Bracegirdle, T. J., & Turner, J. (2016). Future circulation changes off West Antarctica: Sensitivity of the Amundsen Sea Low to projected anthropogenic forcing. *Geophysical Research Letters*, *43*, 367–376. https://doi.org/10.1002/2015GL067143

Hosking, J. S., Orr, A., Marshall, G. J., Turner, J., & Phillips, T. (2013). The influence of the Amundsen-Bellingshausen Seas Low on the climate of West Antarctica and its representation in coupled climate model simulations. *Journal of Climate*, *26*(17), 6633–6648. https://doi.org/10.1175/JCLI-D-12-00813.1

Jackett, D., & McDougall, T. (1997). A neutral density variable for the world's ocean. *Journal of Physical Oceanography*, *27*(2), 237–263. https://doi.org/10.1175/1520-0485(1997)027<0237:ANDVFT>2.0.CO;2

Jacobs, S., Jenkins, A., Giulivi, C., & Dutrieux, P. (2011). Stronger ocean circulation and increased melting under Pine Island Glacier ice shelf. *Nature Geoscience*, *4*, 519–523. https://doi.org/10.1038/ngeo1188

Jenkins, A., Dutrieux, P., Jacobs, S., Steig, E. J., Gudmundsson, G. H., Smith, J., & Heywood, K. J. (2016). Decadal ocean forcing and Antarctic ice sheet response: Lessons from the Amundsen Sea. *Oceanography*, *29*(4), 106–117. https://doi.org/10.5670/oceanog.2016.103

Jenkins, A., Dutrieux, P., Jacobs, S. S., McPhail, S. D., Perrett, J. R., Webb, A. T., & White, D. (2010). Observations beneath Pine Island Glacier in West Antarctica and implications for its retreat. *Nature Geoscience*, *3*(7), 468–472. https://doi.org/10.1038/ngeo890

Jenkins, A., Shoosmith, D., Dutrieux, P., Jacobs, S., Kim, T. W., Lee, S. H., et al. (2018). West Antarctic Ice Sheet retreat in the Amundsen Sea driven by decadal oceanic variability. *Nature Geoscience*, *11*(10), 733–738. https://doi.org/10.1038/s41561-018-0207-4

Johnson, J. A., & Killworth, P. D. (1975). A bottom current along the shelf break. *Journal of Physical Oceanography*, *5*(1), 185–188. https://doi.org/10.1175/1520-0485(1975)005<0185:ABCATS>2.0.CO;2

Joughin, I., Smith, B. E., & Medley, B. (2014). Marine ice sheet collapse potentially under way for the Thwaites Glacier Basin, West Antarctica. *Science*, *344*(6185), 735–738. https://doi.org/10.1126/science.1249055

Kalén, O., Assmann, K. M., Wåhlin, A. K., Ha, H. K., Kim, T. W., & Lee, S. H. (2016). Is the oceanic heat flux on the central Amundsen Sea shelf caused by barotropic or baroclinic currents? *Deep Sea Research Part II*, *123*, 7–15. https://doi.org/10.1016/j.dsr2.2015.07.014

Kim, T. W., Ha, H. K., Wåhlin, A. K., Lee, S. H., Kim, C. S., Lee, J. H., & Cho, Y. K. (2017). Is Ekman pumping responsible for the seasonal variation of warm circumpolar deep water in the Amundsen Sea? *Continental Shelf Research*, *132*, 38–48. https://doi.org/10.1016/j.csr.2016.09.005

Kimura, S., Jenkins, A., Regan, H., Holland, P. R., Assmann, K. M., Whitt, D. B., et al. (2017). Oceanographic controls on the variability of ice-shelf basal melting and circulation of glacial meltwater in the Amundsen Sea Embayment, Antarctica. *Journal of Geophysical Research: Oceans*, *122*, 10,131–10,155. https://doi.org/10.1002/2017JC012926

Klinck, J. M. (1996). Circulation near submarine canyons: A modeling study. *Journal of Geophysical Research*, *101*(C1), 1211–1223. https://doi.org/10.1029/95JC02901

Konrad, H., Shepherd, A., Gilbert, L., Hogg, A., McMillan, M., Muir, A., & Slater, T. (2018). Net retreat of Antarctic glacier grounding lines. *Nature Geoscience*, *11*(4), 258–262. https://doi.org/10.1038/s41561-018-0082-z

Lachlan-Cope, T., & Connolley, W. (2006). Teleconnections between the tropical Pacific and the Amundsen-Bellinghausens Sea: Role of the El Niño/Southern Oscillation. *Journal of Geophysical Research*, *111*, D23101. https://doi.org/10.1029/2005JD006386

Large, W. G., McWilliams, J. C., & Doney, S. (1994). Oceanic vertical mixing: A review and a model with a nonlocal boundary layer parameterization. *Reviews of Geophysics*, *32*(4), 363–403. https://doi.org/10.1029/94RG01872

Lill, C. C. (1979). Upwelling over the shelf break. *Journal of Physical Oceanography*, *9*(5), 1044–1047. https://doi.org/10.1175/1520-0485(1979)009<1044:UOTSB>2.0.CO;2

Locarnini, R. A., Mishonov, A. V., Antonov, J. I., Boyer, T. P., Garcia, H. E., Baranova, O. K., et al. (2010). World ocean atlas 2009, volume 1: Temperature. In S. Levitus (Ed.), *NOAA Atlas NESDIS 68* (p. 184). Washington, DC: U.S. Government Printing Office.

Losch, M. (2008). Modeling ice shelf cavities in a z coordinate ocean general circulation model. *Journal of Geophysical Research*, *113*, C08043. https://doi.org/10.1029/2007JC004368

Losch, M., Menemenlis, D., Campin, J.-M., Heimbach, P., & Hill, C. (2010). On the formulation of sea-ice models. Part 1: Effects of different solver implementations and parameterizations. *Ocean Modelling*, *33*(1-2), 129–144. https://doi.org/10.1016/j.ocemod.2009.12.008

Marshall, G. (2003). Trends in the Southern Annular Mode from observations and reanalyses. *Journal of Climate*, *16*(24), 4134–4143. https://doi.org/10.1175/1520-0442(2003)016<4134:TITSAM>2.0.CO;2

McDougall, T.J., & Barker, P. M. (2011). Getting started with TEOS-10 and the Gibbs Seawater (GSW) Oceanographic Toolbox. SCOR/IAPSO WG127, 28pp., ISBN 978-0-646-55621-5.

Morlighem, M., Rignot, E., Binder, T., Blankenship, D., Drews, R., Eagles, G., et al. (2020). Deep glacial troughs and stabilizing ridges unveiled beneath the margins of the Antarctic ice sheet. *Nature Geoscience*, *13*(2), 132–137. https://doi.org/10.1038/s41561-019-0510-8

Mouginot, J., Rignot, E., & Scheuchl, B. (2014). Sustained increase in ice discharge from the Amundsen Sea Embayment, West Antarctica, from 1973 to 2013. *Geophysical Research Letters*, *41*, 1576–1584. https://doi.org/10.1002/2013GL059069

Nakayama, Y., Menemenlis, D., Zhang, H., Schodlok, M., & Rignot, E. (2018). Origin of Circumpolar Deep Water intruding onto the Amundsen and Bellingshausen Sea continental shelves. *Nature Communications*, *9*(1), 3403. https://doi.org/10.1038/s41467-018-05813-1

Nakayama, Y., Timmermann, R., Rodehacke, C. B., Schröder, M., & Hellmer, H. H. (2014). Modeling the spreading of glacial meltwater from the Amundsen and Bellingshausen seas. *Geophysical Research Letters*, *41*, 7942–7949. https://doi.org/10.1002/2014GL061600

Paolo, F. S., Fricker, H. A., & Padman, L. (2015). Volume loss from Antarctic ice shelves is accelerating. *Science*, *348*(6232), 327–331. https://doi.org/10.1126/science.aaa0940

Peacock, N. R., & Laxon, S. W. (2004). Sea surface height determination in the Arctic Ocean from ERS altimetry. *Journal of Geophysical Research*, *109*, C07001. https://doi.org/10.1029/2001JC001026

Raphael, M. N., Marshall, G. J., Turner, J., Fogt, R. L., Schneider, D., Dixon, D. A., et al. (2016). The Amundsen Sea Low: Variability, change, and impact on Antarctic climate. *Bulletin of the American Meteorological Society*, *97*(1), 111–121. https://doi.org/10.1175/BAMS-D-14-00018.1

Rayner, N. A., Parker, D. E., Horton, E. B., Folland, C. K., Alexander, L. V., Rowell, D. P., et al. (2003). Global analyses of sea surface temperature, sea ice, and night marine air temperature since the late nineteenth century. *Journal of Geophysical Research*, *108*(D14), 4407. https://doi.org/10.1029/2002JD002670

Rignot, E., Mouginot, J., Morlighem, M., Seroussi, H., & Scheuchl, B. (2014). Widespread, rapid grounding line retreat of Pine Island, Thwaites, Smith, and Kohler glaciers, West Antarctica, from 1992 to 2011. *Geophysical Research Letters*, *41*, 3502–3509. https://doi.org/10.1002/2014GL060140

Shepherd, A., Ivins, E., Rignot, E., Smith, B., van den Broeke, M., Velicogna, I., et al. (2018). Mass balance of the Antarctic Ice Sheet from 1992 to 2017. *Nature*, *558*(7709), 219–222. https://doi.org/10.1038/s41586-018-0179-y

Silvano, A., Rintoul, S. R., Kusahara, K., Peña-Molino, B., van Wijk, E., Gwyther, D. E., & Williams, G. D. (2019). Seasonality of warm water intrusions onto the continental shelf near the Totten Glacier. *Journal of Geophysical Research: Oceans*, *124*, 4272–4289. https://doi.org/10.1029/2018JC014634

Spence, P., Griffies, S. M., England, M. H., Hogg, A. M. C., Saenko, O. A., & Jourdain, N. C. (2014). Rapid subsurface warming and circulation changes of Antarctic coastal waters by poleward shifting winds. *Geophysical Research Letters*, *41*, 4601–4610. https://doi.org/10.1002/2014GL060613

Spence, P., Holmes, R. M., Hogg, A. M., Griffies, S. M., Stewart, K. D., & England, M. H. (2017). Localized rapid warming of West Antarctic subsurface waters by remote winds. *Nature Climate Change*, *7*(8), 595–603. https://doi.org/10.1038/NCLIMATE3335

Steig, E. J., Ding, Q., Battisti, D. S., & Jenkins, A. (2012). Tropical forcing of Circumpolar Deep Water inflow and outlet glacier thinning in the Amundsen Sea Embayment, West Antarctica. *Annals of Glaciology*, *53*(60), 19–28. https://doi.org/10.3189/2012AoG60A110

St-Laurent, P., Klinck, J. M., & Dinniman, M. S. (2013). On the role of coastal troughs in the circulation of warm circumpolar deep water on Antarctic shelves. *Journal of Physical Oceanography*, *43*(1), 51–64. https://doi.org/10.1175/JPO-D-11-0237.1

St-Laurent, P., Klinck, J. M., & Dinniman, M. S. (2015). Impact of local winter cooling on the melt of Pine Island Glacier, Antarctica. *Journal of Geophysical Research: Oceans*, *120*, 6718–6732. https://doi.org/10.1002/2015JC010709

Thoma, M., Jenkins, A., Holland, D., & Jacobs, S. (2008). Modelling Circumpolar Deep Water intrusions on the Amundsen Sea continental shelf, Antarctica. *Geophysical Research Letters*, *35*, L18602. https://doi.org/10.1029/2008GL034939

Thompson, A. F., Stewart, A. L., Spence, P., & Heywood, K. J. (2018). The antarctic slope current in a changing climate. *Reviews of Geophysics*, *56*, 741–770. https://doi.org/10.1029/2018RG000624

Thyng, K. M., Greene, C. A., Hetland, R. D., Zimmerle, H. M., & DiMarco, S. F. (2016). True colors of oceanography: Guidelines for effective and accurate colormap selection. *Oceanography*, *29*(3), 9–13. https://doi.org/10.5670/oceanog.2016.66

Timmermann, R., Le Brocq, A., Deen, T., Domack, E., Dutrieux, P., Galton-Fenzi, B., et al. (2010). A consistent data set of Antarctic ice sheet topography, cavity geometry, and global bathymetry. *Earth System Science Data*, *2*(2), 261–273. https://doi.org/10.5194/essd-2-261-2010

Turner, J., Hosking, J. S., Bracegirdle, T. J., Phillips, T., & Marshall, G. J. (2017). Variability and trends in the Southern Hemisphere high latitude, quasi-stationary planetary waves. *International Journal of Climatology*, *37*(5), 2325–2336. https://doi.org/10.1002/joc.4848

Turner, J., Phillips, T., Hosking, J. S., Marshall, G. J., & Orr, A. (2013). The Amundsen Sea Low. *International Journal of Climatology*, *33*(7), 1818–1829. https://doi.org/10.1002/joc.3558

Wåhlin, A. K., Kalen, O., Arneborg, L., Björk, G., Carvajal, G. K., Ha, H. K., et al. (2013). Variability of warm deep water inflow in a submarine trough on the Amundsen shelf. *Journal of Physical Oceanography*, *43*(10), 2054–2070. https://doi.org/10.1175/JPO-D-12-0157.1

Wåhlin, A. K., Muench, R. D., Arneborg, L., Björk, G., Ha, H. K., Lee, S. H., & Alsén, H. (2012). Some implications of Ekman layer dynamics for cross-shelf exchange in the Amundsen Sea. *Journal of Physical Oceanography*, *42*(9), 1461–1474. https://doi.org/10.1175/JPO-D-11-041.1

Walker, D. P., Jenkins, A., Assmann, K. M., Shoosmith, D. R., & Brandon, M. A. (2013). Oceanographic observations at the shelf break of the Amundsen Sea. *Journal of Geophysical Research: Oceans*, *118*, 2906–2918. https://doi.org/10.1002/JGRC.20212

Webb, D. J., Holmes, R. M., Spence, P., & England, M. H. (2019). Barotropic Kelvin wave-induced bottom boundary layer warming along the West Antarctic Peninsula. *Journal of Geophysical Research: Oceans*, *124*, 1595–1615. https://doi.org/10.1029/2018JC014227

Webber, B. G., Heywood, K. J., Stevens, D. P., & Assmann, K. M. (2019). The impact of overturning and horizontal circulation in Pine Island trough on ice shelf melt in the eastern Amundsen Sea. *Journal of Physical Oceanography*, *49*(1), 63–83. https://doi.org/10.1175/JPO-D-17-0213.1

Webber, B. G., Heywood, K. J., Stevens, D. P., Dutrieux, P., Abrahamsen, E. P., Jenkins, A., et al. (2017). Mechanisms driving variability in the ocean forcing of Pine Island Glacier. *Nature Communications*, *8*(1), 14,507. https://doi.org/10.1038/ncomms14507